NASA Technical Memorandum 84289

NASA-TM-84289 19830009281

Minimum-Fuel Turning Climbout and Descent Guidance of Transport Jets

F. Neuman and E. Kreindler

January 1983

National Aeronautics and
Space Administration

NASA Technical Memorandum 84289

Minimum-Fuel Turning Climbout and Descent Guidance of Transport Jets

F. Neuman, Ames Research Center, Moffett Field, California
E. Kreindler, E. E. Technion, Israel Institute of Technology, Haifa, Israel

National Aeronautics and
Space Administration

Ames Research Center
Moffett Field, California 94035

MINIMUM-FUEL TURNING CLIMBOUT AND DESCENT GUIDANCE OF TRANSPORT JETS

F. Neuman and E. Kreindler*

Ames Research Center

SUMMARY

The complete flightpath optimization problem for minimum fuel consumption from takeoff to landing including the initial and final turns from and to the runway heading is solved. However, only the initial and final segments which contain the turns are treated, since the straight-line climbout, cruise, and descent problems have already been solved. The paths are derived by generating fields of extremals, using the necessary conditions of optimal control together with singular arcs and state constraints. Results show that the speed profiles for straight flight and turning flight are essentially identical except for the final horizontal accelerating or decelerating turns. The optimal turns require no abrupt maneuvers, and an approximation of the optimal turns could be easily integrated with present straight-line climb-cruise-descent fuel-optimization algorithms. Climbout at the optimal IAS rather than the 250-knot terminal-area speed limit would save 36 lb of fuel for the 727-100 aircraft.

INTRODUCTION

The escalating costs of fuel have increasingly focused attention on the problem of minimizing fuel consumption of commercial aircraft. Recent work in aircraft guidance has demonstrated that onboard optimization of aircraft trajectories offers an efficient method of fuel conservation.

Aircraft trajectory-minimum fuel problems can be divided into two classes: en route problems, with trajectory lengths of 50 n. mi. and longer; and terminal-area problems with lengths of 3 to 50 n. mi. For the en route problem, an onboard algorithm for optimum climb-cruise-descent has been developed by applying optimal control theory (ref. 1). The solution was developed for the vertical plane only, since horizontal maneuvers are not a significant feature of en route flight.

The general class of terminal-area trajectory problems are more difficult to solve, because vertical and horizontal maneuvers involving speed, altitude, and heading changes occur simultaneously and because they are of comparable significance in influencing fuel consumption.

In this report we study the subclass of terminal-area climbout and descent trajectories which are part of an overall optimal trajectory that includes an en route straight-line optimal cruise segment. These maneuvers complete the optimal cruise trajectory problem of reference 1 by including the initial and final turns from and

---

*Professor at E. E. Technion, Israel Institute of Technology, Haifa, Israel.

to runway headings. For this subclass of terminal-area problems, essentially all possible extremals can be found, and the problem of global optimality encountered in the general class of terminal-area turning flightpaths can be resolved (ref. 2).

The results presented in this paper show that for fuel-efficient turning climbout and descent guidance, the altitude-speed profile is nearly the same as that generated for straight-line flightpaths. In the special case of straight-line flightpaths, the results presented in this paper are identical to those presented in reference 1.

Further research is needed on a second class of problems, that of optimal capture trajectories. These are trajectories which end by aligning the aircraft with the Instrument Landing System (ILS) localizer at a specific point and heading and begin at any other point and heading. These problems arise especially in the descent phase when the aircraft does not arrive in the terminal area at the proper state to complete an optimal approach or, for air-traffic-control reasons, is not permitted to complete the optimal maneuver. The approach in previous studies has been to synthesize and sometimes optimize vertical (ref. 1) and horizontal trajectories (refs. 3-6) separately and then combine them heuristically (refs. 7-9). In further research one can use extremals to study samples of optimal three-dimensional trajectories, which include speed changes, and thus verify and refine existing heuristic solutions. However, this problem is not addressed in this paper.

PROBLEM STATEMENT

The problem is to minimize the fuel consumption over the complete flightpath from takeoff to touchdown, F_T. In order to solve this problem, the equations of motion for the vehicle are needed and the performance index must be formulated.

The point-mass equations of motion for an aircraft in steady-state flight (weight = lift/cos ϕ), assuming small flightpath angle, constant mass, and coordinated turns are:

$$\dot{x} = v \cos \psi \tag{1}$$

$$\dot{y} = v \sin \psi \tag{2}$$

$$\dot{h} = v\gamma \tag{3}$$

$$\dot{\psi} = -gu/v \tag{4}$$

$$\dot{v} = g(T - D - W\gamma)/W \tag{5}$$

Here, x and y are the coordinates in the horizontal plane, h is the vertical coordinate, ψ is the heading angle measured counterclockwise from the x-axis, v is the ground speed, g is the gravitational constant, W is the weight, and D is the drag. The control variables are:

1. Thrust, T, where thrust is constrained to be between idle and maximum allowable thrust:

$$T_{idle} \leq T \leq T_{max}$$

2. Flightpath angle, γ, which is constrained in accordance with present commercial airline practice:

$$\gamma_{min} \leq \gamma \leq \gamma_{max}$$

$$\gamma_{min} = 0°, \ \gamma_{max} = 5° \quad \text{for climbout}$$

$$\gamma_{min} = -4°, \ \gamma_{max} = 0° \quad \text{for descent}$$

3. The tangent of the bank angle, u, which is constrained in accordance with present practice for commercial autopilots.

$$-u_m \leq u \leq u_m \qquad u_m = \tan \phi, \quad \phi = 30°$$

The only state constraint that was applied was on airspeed. FAA regulations state that the indicated airspeed in the terminal area must not exceed $v_I = 250$ knots (422 ft/sec); when converted into true airspeed (which is equal to the ground speed in the assumed no-wind condition) this translates into a state variable constraint for the speed v:

$$S = v - v_I(1 + qh) \leq 0; \quad v_I = 422 \text{ ft/sec}; \quad q = 0.162 \times 10^{-4} \tag{6}$$

The next problem is to develop the performance index for the low-altitude turning segment. This requires some preliminary discussion of various approximations. The intended solution for the complete minimal-fuel turning flightpath is to connect the optimal solution for the straight-line flightpath from reference 1 (cut off below an altitude of 10,000 ft) with an optimal turning climbout and descent (connected to the straight-line path at the 10,000-ft altitude). From Bellman's principle of optimality (ref. 10) it can be said that "any portion of an optimal trajectory is also optimal." However, the converse of piecing together portions of optimal trajectories will result in an optimal trajectory only under rather special conditions. But this piecing is precisely what we intend to do. It will be shown, from the numerical results, that piecing together a straight-line, optimal, high-altitude trajectory with a turning low-altitude trajectory will be an extremely close approximation of an optimal flightpath.

The first approximation is that the high-altitude portion of a long-distance optimal flightpath is a straight line in the horizontal plane. In reference 6 it was shown that for optimal horizontal flightpaths that involve initial and final turns, the flightpath does not contain a mathematically straight-line portion. However, even for flightpaths as short as 20 n. mi. there is a center portion of the flightpath that is straight for all practical purposes. Then, for the much longer flightpaths considered here, the assumption of a straight-line horizontal projection of the center portion of the trajectory appears reasonable. If, in addition, the initial portion of the turning descent is also almost a straight line and the speeds and controls at the junction match, so that there is no discontinuity, then one can be reasonably assured that the joining of the path segments will result in a close approximation of a fuel-optimal flightpath.

In order to develop the performance index, F_T, it is convenient to refer to figure 1 where the flightpath has been drawn to include a turning climbout segment from t_1 to 10,000-ft altitude (t_2), a straight-line climbing segment (R_{CLIMB}), from t_2 to cruise altitude, a straight-line cruise segment (R_{CRUISE}), a straight-line

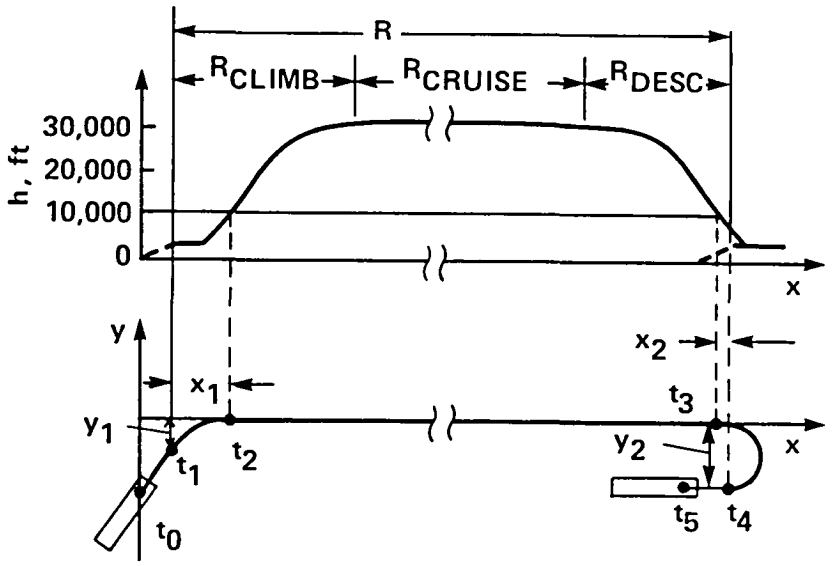

Figure 1.- Optimal flightpath. Note: $t_0 - t_1$ and $t_4 - t_5$ are not subject to optimization.

descending segment ($R_{DESCENT}$) from cruise altitude to 10,000-ft altitude (t_3), and a turning descent from 10,000-ft altitude to the final approach fix t_4. For a given stage length R, the optimal cruise altitude and speed change very little with minor changes in the length of the straight flightpath $R_{CRUISE} + R_{CLIMB} + R_{DESCENT}$ that may occur when considering alternative low-altitude climbouts and descents. Any change is primarily reflected in the change of the cruise distance, while the high-altitude climb and descent strategies are not affected. This means that the optimal fuel consumed during the straight-line climbout and descent segments is independent of the rest of the flightpath and can therefore be represented by a constant and the fuel consumed during the cruise segment is directly proportional to the range traveled at cruise altitude; then the total fuel consumed during the flight can be expressed by the equation

$$F_T = \int_{t_1}^{t_2} F\,dt + CR_{CRUISE} + \int_{t_3}^{t_4} F\,dt + K_1 \tag{7}$$

where F is fuel burn rate, C is the fuel per nautical mile expended at optimal cruise speed and altitude (ref. 1), K_1 is the fuel consumed during the optimal straight-line climb and descent segments of flight, and R_{CRUISE} is the distance traveled at cruise. From figure 1 it is seen that

$$R_{CRUISE} = R - R_{CLIMB} - R_{DESCENT} - x_1 - x_2$$

where R (the distance between the climbout fix and final-approach fix), R_{CLIMB}, and $R_{DESCENT}$ are constants. (Referring to fig. 1, we realize that y_1 and y_2 have negligible effect on the length of the long-distance straight-line flightpath above an altitude of 10,000 ft.) We define x_1 and x_2 to be:

$$x_1 = \int_{t_1}^{t_2} v\cos\psi\,dt\ ; \qquad x_2 = \int_{t_3}^{t_4} v\cos\psi\,dt$$

so that

$$F_T = \int_{t_1}^{t_2} (F - Cv\cos\psi)dt + \int_{t_3}^{t_4} (F - Cv\cos\psi)dt + K_1 + K_2$$

where

$$K_2 = C(R - R_{CLIMB} - R_{DESCENT})$$

Therefore, provided that the overall flightpath is long enough to have a cruise segment, the performance function applicable to the low-altitude climb/descent portions of the complete flightpath has two parts and equals the fuel expended in the ascent (descent) minus the fuel saved by shortening the cruising portion of the high-altitude flightpath:

$$J = \int_{t_1(t_3)}^{t_2(t_4)} (F - Cv \cos \psi)dt \tag{8}$$

The upper and lower limits of integration are those appropriate for ascent (t_1 and t_2), and descent (t_3 and t_4), respectively, and the upper limit of integration is free.

The initial and final states for descent are:

$$h_o = 10{,}000 \text{ ft}$$

$$\psi_o = 0$$

$$v(0) \leq 250 \text{ knots IAS}$$

$$h_f = 2000 \text{ ft}$$

$$v_f = 180 \text{ knots}$$

and ψ_f is specified between 0 and π. The values are reversed for ascent. The values for (x_1,y_1) and (x_2,y_2) of figure 1 are not specified. The terminal altitude h_f and speed v_f are chosen to permit a final straight-in landing approach along a specified glide slope. The initial speed $v(0)$ is either determined by the speed constraint or, if the speed constraint is not violated, by the speed dictated when flying the solution of the optimization problem. Numerical results show that the terminal conditions at 10,000-ft altitude are the proper initial and final conditions for the straight en route portion of the flightpath.

In order to solve the minimum-fuel climbout and descent problems it is necessary to model the drag, thrust, and fuel-flow rate for a specific aircraft. Choosing the Boeing 727-100 as an example, the drag, D, is modeled by

$$D = D_1 + D_2 u^2 \tag{9a}$$

where the drag for nonturning flight, D_1, is given by

$$D_1 = k_1(1 + k_2 h) + k_3(1 + k_4 h)v^2 + k_5(1 + k_6 h)/v^2 \tag{9b}$$

and the bank-angle-induced drag, D_2, is given by

$$D_2 = k_1(1 - k_2 h)/2 + k_5(1 + k_6 h)/v^2 \tag{9c}$$

This approximation for drag results in a minimum drag of 9000 lb and includes sufficient flap deployment at the lower speeds such that an 8° angle of attack is not exceeded. In general, takeoff and landing weights differ from the nominal W = 150,000 lb. In this case, k_1 is multiplied by (W/150,000) and k_5 by $(W/150{,}000)^2$ to provide a reasonable approximation of the drag.

The thrust value T_{max} was chosen to be 23,000 lb and T_{idle} was set equal to zero. Both the maximum and minimum or idle thrust values are altitude- and speed-dependent. The idle thrust is small enough to be negligible. To simplify this analysis, the maximum allowable thrust has been chosen as the smallest maximum value allowable over the altitude range of 0 to 10,000 ft.

The fuel flow rate for the 727-100 is modeled by

$$F = C_0 + C_1 T + C_2 T^2 \tag{10}$$

where

$$C_j = c_{4j+1}(1 + c_{4j+2}h) + c_{4j+3}(1 + c_{4j+4}h)v; \qquad j = 0, 1, 2 \tag{11}$$

and the numerical values of the k's and c's are provided in appendix A.

The optimal cruise fuel used per nautical mile, C, was set equal to 17.5 lb/n. mi., which was obtained from reference 1. This particular C is for the example of a 200-n. mi. flight with a takeoff weight of 150,000 lb. This number will change for other weights and distances. We are interested here only in the character of the optimal turning climb and descent, and therefore do not change C or W in our computations. However, if optimization of a specific path was required, one would first optimize the straight-line path between airports and obtain C as well as takeoff and landing weights. This information would be accurate enough to compute the turning terminal-area paths without resorting to iteration.

THE NECESSARY CONDITIONS

In this particular optimal control, which requires the capturing of a specific heading, the state variables x and y in equations (1) and (2) can be ignored (hence, we do not have λ_x and λ_y in the Hamiltonian); they are required, of course, for the flight trajectories in the horizontal plane.

For our analysis, we make the following assumptions, which are true for the numerical values of this problem.

Assumption 1. For the applicable range of velocities, available thrust exceeds the aircraft drag. This can be seen from figure 3 of appendix A where $0 < D(v,h) < T_{max}$.

Assumption 2. The fuel flow rate at $T_{min} = 0$ is positive, which eliminates the consideration of gliding flightpaths with shut-off engines. Also, $T_{min} > -C_1(v,h)/[2C_2(v,h)]$ for all v and h. This is significant for the calculation of the extremal thrust.

The Hamiltonian for this problem is

$$\begin{aligned} H &= F + \lambda^T f + \eta S \\ &= C_0 + C_1 T + C_2 T^2 - Cv\cos\psi + \lambda_h v\gamma - \lambda_\psi gu/v \\ &\quad + \lambda_v g(T - D_1 - D_2 u^2 - W\gamma)/W + \eta[v - v_I(1 + qh)] \end{aligned} \tag{12}$$

where $\eta \geq 0$, $\eta(v - v_I(1 - qh) \equiv 0$ (ref. 11), and the convention of normalizing the costate variables by setting the costate variable, λ_0, which multiplies the performance function, to one is applied. The the remaining costate variables are given by

$$\dot{\lambda}_h = -H_h = -C_{0_h} - C_{1_h}T - C_{2_h}T^2 + \lambda_v g(D_{1_h} + D_{2_h}u^2)/W + \eta v_I q \tag{13}$$

$$\dot{\lambda}_\psi = -H_\psi = Cv \sin \psi \tag{14}$$

$$\dot{\lambda}_v = -H_v = -C_{0_v} - C_{1_v}T - C_{2_v}T^2 - C \cos \psi - \lambda_h \gamma - \lambda_\psi gu/v^2$$

$$+ \lambda_v g(D_{1_v} + D_{2_v}u^2)/W - \eta \tag{15}$$

where $H_h = \partial H/\partial h$, and $C_{0_h} = \partial C_0/\partial h$, etc. Since t_f is not prescribed and $H_t = 0$, then,

$$H \equiv 0, \text{ for all } t \in [0,t_f] \tag{16}$$

It is noted that in our approach the cruise cost C is part of the Hamiltonian, due to the performance index. The Hamiltonian would be identical if the fuel consumed had been the only variable used as performance index and if the values $\lambda_x = C$ and $\lambda_y = 0$ had been chosen. This observation ties the present work to reference 1, where the cruise cost λ is the only adjoint variable and $\lambda^* = C$ is the optimal cruise cost for a particular flightpath.

Finding the argument of H, namely T, that minimizes H while using the permissible range of T yields the extremal thrust, $T^* = \arg \min_T H$

$$T^* = \begin{cases} T_{max} & \text{if} \quad \tau \geq T_{max} \\ \tau & \text{if} \quad T_{min} < \tau < T_{max} \\ T_{min} & \text{if} \quad \tau \leq T_{min} \end{cases} \tag{17}$$

where

$$\tau = -(C_1 + \lambda_v g/W)/(2C_2) \tag{18}$$

and C_1 and C_2 are functions of h and v. Since minimization of H yields T^* uniquely, it can be shown (see ref. 11) that T^* and λ_v are continuous at junction times between the velocity-constrained and the unconstrained arcs. Thus thrust is seen to be a continuous function of λ_v and t. Since C_2 is small for all h and v, the range of λ_v for intermediate thrust is narrow and, as we shall see in the Results section of this paper, intermediate thrust will not occur for the optimal turning descents and climbouts.

We observe that equations (4) and (14) imply that

$$u = 0 \quad \text{if} \quad \lambda_\psi = 0 \text{ on an interval} \tag{19}$$

This is true irrespective of the minimization of H with respect to u. From the latter we obtain, by using $H_u = 0$ and $H_{uu} > 0$,

$$u^* = \begin{cases} \nu & \text{if} \quad |\nu| < u_m \quad \text{and} \quad \lambda_v < 0 \\ u_m \text{ sgn } \nu & \text{if} \quad |\nu| \geq u_m \quad \text{and} \quad \lambda_v < 0 \end{cases} \tag{20}$$

where

$$\nu = -(\lambda_\psi W)/(2\lambda_v D_2 v) \tag{21}$$

If $\lambda_v \geq 0$ and λ_ψ does not vanish on an interval (denoted by $\lambda_\psi \equiv 0$), the minimization of H gives

$$u^* = u_m \text{ sgn } \lambda_\psi \; ; \qquad \lambda_v \geq 0 \quad \text{and} \quad \lambda_\psi \not\equiv 0 \tag{22}$$

We note that λ_v cannot be positive while λ_ψ vanishes on an interval because then minimization of H implies $u^* = \pm u_m$, which is incompatible with equation (19). However, if λ_ψ vanishes on an interval and λ_v crosses from negative to positive values, say at $t = t_2$, then u switches from $u(t) = 0$, $t < t_2$ to $u(t_2^+) = \pm u_m$, dependent on λ_ψ, which is no longer zero. This is a transition from a straight-line flightpath to a curved one. Such discontinuous bank angle would have to occur at zero thrust, thus it might occur (but actually did not occur) after initiation of the optimal descent.

Lastly we evaluate the flightpath angle γ. Since we have chosen to work with small angles ($\sin \gamma = \gamma$, $\cos \gamma = 1$), γ appears linearly in the equations. Therefore, γ will either be at its limits based on the minimization of H, from $\gamma^* = \arg \min_\gamma H$

$$\gamma^* = \begin{cases} \gamma_{max} & \text{if} \quad H_\gamma < 0 \\ \gamma_{min} & \text{if} \quad H_\gamma > 0 \end{cases} \tag{23}$$

where

$$H_\gamma = \lambda_h v - \lambda_v g$$

or

$$H_\gamma = \lambda_h v - \lambda_v g = 0 \Rightarrow \lambda_h = \lambda_v g/v \quad \text{on a subinterval} \tag{24}$$

in which case γ will form a singular arc. In addition, when the speed constraint is reached, γ is used to control speed. These latter two cases, where γ will form a singular arc and where velocity is on the speed constraint, are covered below in more detail.

Flightpath Guidance Along a Singular-γ Arc

When flying along a singular-γ arc, equation (24) implies that all time derivatives of H_γ vanish.

$$(\dot{H}_\gamma) = \dot{\lambda}_h v + \lambda_h \dot{v} - \dot{\lambda}_v g = 0 \tag{25}$$

Solution of the simultaneous equations for $H = 0$ and $\dot{H}_\gamma = 0$ permit the calculation of the adjoint variables λ_v and λ_ψ. For simplicity, λ_v and λ_ψ are calculated under the assumption (to be verified) that $T = T_{max}$ = constant for optimal climbout and $T = T_{min}$ = constant for optimal descent. There are three cases for u: $u = 0$, $u = u_m$ (maximum), and $-u_m < u < u_m$ (intermediate). We then examine the equations numerically to check whether they are consistent with the assumption (e.g., λ_v must be in the appropriate range for the assumed T, v must be in the speed range of interest, and the λ's must be real numbers). The singular arc flightpath profiles, γ_A, are calculated for those cases where the singular arc is found possible. The singular arc can be found as follows. By using (24) in the equation for $H = 0$ (12) the dependence of (12) on γ is eliminated. The additional assumption is made that the solution is not bounded by the speed constraint, $\eta = 0$. In addition, by substituting $\dot{\lambda}_h$ from (13), $\dot{\lambda}_v$ from (15), $\dot{v}$ from (5), and λ_h from (24) into (25), and by placing $H = 0$ and $\dot{H}_\gamma = 0$, we have three equations with three unknowns u, λ_v, and λ_ψ.

$$\left.\begin{aligned} 2H/v \Rightarrow \lambda_v(A_x + B_x u^2) - \lambda_\psi C_x u + D_x &= 0 \\ \dot{H}_\gamma/g - H/v \Rightarrow \lambda_v(E_x + P_x u^2) + \lambda_\psi C_x u + G_x &= 0 \\ u = H_x \lambda_\psi/\lambda_v\Big|_{|u|<u_m} & \end{aligned}\right\} \qquad (26a)$$

with the following coefficients

$$\left.\begin{aligned} A_x &= 2g(T - D_1)/(vW) \\ B_x &= -2gD_2/(vW) \\ C_x &= 2g/v^2 \\ D_x &= 2F/v - 2C\cos\psi \\ E_x &= D_{1_h} v/W - gD_{1_v}/W \\ P_x &= D_{2_h} v/W - D_{2_v} g/W \\ G_x &= -F/v - F_h v/g + F_v \\ H_x &= -W/(2D_2 v) \end{aligned}\right\} \qquad (26b)$$

Solving equations (26) for λ_v and λ_ψ with $|u| < u_m$

$$\lambda_v = [D_x(P_x H_x + C_x) - G_x(B_x H_x - C_x)]/[E_x(B_x H_x - C_x) - A_x(P_x H_x + C_x)] \qquad (27)$$

$$\lambda_\psi = \lambda_c \sqrt{(G_x A_x - D_x E_x)/\{H_x[D_x(P_x H_x + C_x) - G_x(B_x H_x - C_x)]\}} \qquad (28)$$

In the special case $u = 0$, from (19),

$$\lambda_\psi = 0 \tag{29}$$

and (26) becomes

$$\lambda_v A_x + D_x = 0 \tag{30a}$$

$$\lambda_v E_x + G_x = 0 \tag{30b}$$

which to be consistent requires

$$G_x A_x - D_x E_x = 0 \tag{31}$$

This is consistent with (28) for $\lambda_\psi = 0$. The variables G_x, A_x, D_x, and E_x are functions of altitude and speed so that we can expect a single altitude-versus-speed profile. If we attempt to obtain an explicit expression for h versus v by expanding (31) we encounter an extremely long polynomial in the 7th power of v and 2nd power of h, which is not very illuminating. We therefore shall be satisfied with a numerical solution of (31). In this case, the altitude-speed profile defines the state space and we do not need to solve $\ddot{H}_\gamma = 0$ to determine γ. Instead, by replacing $\dot{h}$ with $\Delta h/\Delta t$ in (3) and $\dot{v}$ with $\Delta v/\Delta t$ in (5) and by dividing the equations and solving for γ, γ can be determined directly from the altitude-speed profile.

$$\gamma = [(T - D_1)/W][(\Delta h/\Delta v)/(\Delta h/\Delta v + v/g)] \tag{32}$$

Solving equation (26) for λ_v and λ_ψ with $|u| = u_m$

$$\lambda_v = -(D_x + G_x)/[(A_x + B_x u_m^2) + (E_x + P_x u_m^2)] \tag{33}$$

and

$$\lambda_\psi = [\lambda_v(A_x + B_x u_m^2) + D_x]/(C_x u_m) \tag{34}$$

This singular case is of little interest for optimum ascents and descents, since $u = u_{max}$ was almost never reached on the singular-γ arc. It should be noted that while λ_v and λ_ψ can be computed directly from the above equations all along the singular-γ arc, it is computationally simpler to use the above equations for computation of initial values only and to integrate (15) to obtain λ_v and (14) to obtain λ_ψ.

The six cases, ascents and descents, each with $u = 0$, $u = u_m$, and $-u_m < u < u_m$, must be checked to determine whether singular arcs are possible. Since the equations are altitude dependent, these cases are checked numerically at $h = 10{,}000$ ft, which is useful for forward integration in descent and backward integration in climb. From the numerical solution of (31), λ_v is obtained from (30a) or (30b). This λ_v, used in (18), is consistent with $T = T_{max}$ for climb and $T = 0$ for descent. For descent the solution of (31) gives a speed below 250 knots IAS, which means that the speed limit will be inactive as required. During the ascent the speed profile along the singular arc crosses above the speed limit. Thus, strictly speaking, ascent on the singular-γ arc is not permitted. However, this case is investigated, since the speed limit in the terminal area may be relaxed by ATC. For $u = u_{max}$, λ_v is consistent

with the assumption for the thrust. Thus singular arc profiles are possible for all u. The above conclusions are identical for all altitudes. Being assured that the singular-γ case is indeed a candidate for an optimal flightpath, the singular arc flightpath for intermediate u is determined from the condition $(\ddot{H}_\gamma) = 0$:

$$\left.\begin{aligned} 0 = (\ddot{H}_\gamma) &= \partial(\dot{H}_\gamma)/\partial t = \partial/\partial t\{-F_h v + \lambda_v[D_h v + g(T - D)/v - gD_v]g/W \\ &\quad + g(F_v - C\cos\psi + \lambda_\psi gu/v^2)\} \\ &= -F_h\dot{v} - \dot{F}_h v + \dot{\lambda}_v[D_h v + g(T - D)/v - gD_v]g/W + \lambda_v[\dot{D}_h v + D_h\dot{v} - g(T - D)\dot{v}/v^2 \\ &\quad - g(D_u\dot{u} + D_h\dot{h} + D_v\dot{v})/v - g\dot{D}_v]g/W \\ &\quad + g(\dot{F}_v + C\sin\psi\dot{\psi} + \dot{\lambda}_\psi gu/v^2 - 2\lambda_\psi gu\dot{v}/v^3 + \lambda_\psi g\dot{u}/v^2) \end{aligned}\right\} \quad (35)$$

For definition of the fuel flow and drag derivatives see appendix B. To solve (35) for γ is straightforward but tedious and will only be sketched out. First, all terms with different time derivatives — $\dot{v}$, $\dot{h}$, $\dot{\psi}$, $\dot{\lambda}_v$, $\dot{\lambda}_\psi$, $\dot{u}$, $\dot{F}_v$, $\dot{F}_h$, $\dot{D}_v$, and $\dot{D}_h$ are combined. The last five time derivatives are eliminated with expressions (B13), (B3), (B5), (B9), and (B11) from appendix B. This results in the following equation for $(\ddot{H}_\gamma)$

$$(\ddot{H}_\gamma) = A_H\dot{v} + B_H\dot{h} + C_H\dot{\psi} + D_H\dot{\lambda}_v + E_H\dot{\lambda}_\psi \quad (36)$$

where the coefficients have the following values:

$$\left.\begin{aligned} A_H &= -F_h + gD_h\lambda_v/W - g^2\lambda_v(T - D)/(Wv^2) - 2g^2\lambda_\psi u/v^3 - g^2\lambda_v D_v/(Wv) \\ &\quad - Q_H(1/v + D_{2_v}/D_2) - vF_{vh} + 2gk_3k_4v^2\lambda_v/W - 2gk_5k_6(1 + u^2)\lambda_v/(Wv^2) \\ &\quad - 2g^2k_3(1 + k_4h)\lambda_v/W - 6\lambda_v g^2k_5(1 + k_6h)(1 + u^2)/(v^4W) \\ B_H &= -g^2\lambda_v D_h/(Wv) - Q_H D_{2_h}/D_2 + gF_{vh} - 2g^2k_3k_4v\lambda_v/W + 2g^2k_5k_6(1 + u^2)\lambda_v/(Wv^3) \\ C_H &= gC\sin\psi \\ D_H &= g(D_h v + g(T - D)/v - gD_v)/W - Q_H/\lambda_v \\ E_H &= g^2u/v^2 + Q_H/\lambda_\psi \\ Q_H &= [g^2\lambda_\psi/v^2 - g^2\lambda_v D_u/(Wv) + (k_1k_2v + 2k_5k_6/v)g\lambda_v u/W \\ &\quad + 4g^2k_5(1 + k_6h)u\lambda_v/(Wv^3)]u \end{aligned}\right\} \quad (37)$$

None of these coefficients involve γ. When the equations for the time derivatives are inserted in (36), γ appears linearly and the solution for γ is

$$\gamma = [A_H g(T - D)/W - C_H gu/v + D_H(-F_v + C\cos\psi - g\lambda_\psi u/v^2 + g\lambda_v D_v/W)$$

$$+ E_H(-Cv\sin\psi)]/[A_H g - B_H v + D_H\lambda_h] \tag{38}$$

For (38) to be a candidate for an optimal solution the generalized Legendre-Clebsch condition must hold

$$(-\ddot{H}_\gamma)_\gamma \geq 0 \rightarrow (-\ddot{H}_\gamma)_\gamma = A_H g - B_H v + D_H\lambda_h > 0 \tag{39}$$

The condition $(-\ddot{H}_\gamma) = 0$ is not possible since (39) is also the denominator for (38), which would imply $\gamma \rightarrow \infty$.

Again we emphasize that the above development applies to the case of constant thrust only since $\partial T/\partial t = 0$ was assumed.

Flightpath Guidance Along the Speed Constraint

Since the climb speed for the singular γ was above the speed constraint we must now develop the equations for γ when flying at the speed constraint, $\eta \neq 0$. Equation (6) is solved for v, which is then differentiated with respect to time and $\dot{h}$ is replaced with (3). Setting the resulting expression for $\dot{v}$ equal to (5), and solving for γ results in the following expression

$$\gamma = [(T - D)/W]\{g/[g + v_I^2 q(1 + qh)]\} \tag{40}$$

where the second factor varies between 0.92 and 0.91 over the altitude range of 10,000 ft. Since $S = 0$ on the speed constraint, equation (6) can be solved for v, and the derivative taken in order to express v and h on the constraint

$$v = v_I(1 + qh) \tag{41a}$$

$$\dot{v} = v_I q\dot{h} \tag{41b}$$

but

$$\dot{h} = v_I(1 + qh)\gamma \tag{41c}$$

which implies

$$\dot{v} = qv_I^2(1 + qh)\gamma \tag{42}$$

Equations (13) and (15) can now be solved for η. In addition, we must satisfy $H_\gamma = 0$, since γ was not determined by this necessary condition. The solution proceeds as follows

$$H_\gamma = 0 = \lambda_h v - \lambda_v g \rightarrow \lambda_h = \lambda_v g/v \tag{43}$$

differentiating equation (43) results in

$$\dot{\lambda}_h = g(v\dot{\lambda}_v - \lambda_v\dot{v})/v^2 \tag{44}$$

Combining equation (44) with equations (13) and (15), we can obtain an expression for η which is not dependent on λ_h or $\dot{\lambda}_v$

$$\eta = \begin{cases} [C_{0_h} + C_{1_h}T + C_{2_h}T^2 - \lambda_v g D_h/W - g(vA_\eta + \lambda_v \dot{v})/v^2]/(v_I q + g/v) \geq 0 & \text{on the constraint} \\ 0 & \text{off the constraint} \end{cases} \tag{45a}$$

where

$$A_\eta \triangleq C_{0_v} + C_{1_v}T + C_{2_v}T^2 - C\cos\psi + \lambda_h\gamma + \lambda_\psi gu/v^2 - \lambda_v g D_v/W \tag{45b}$$

In (45) v and $\dot{v}$ are given by (41a) and (42).

To complete the statement of the necessary conditions, the character of the velocity set must be studied. The above results may be suspect, since the velocity set for this problem ($\dot{v}$, $\dot{\psi}$, $\dot{h}$, F) is not convex everywhere. However, it is shown in appendix C that the nonconvexity of the velocity set may be ignored for this minimum-fuel problem.

COMPUTATION OF EXTREMALS

The extremals are computed by numerical integration of the state and costate equations (1)-(5) and (13)-(15) with the control T given by (17)-(18), u given by (19)-(22), and γ given by (23) or (38) on the singular-γ arc or by (40) when the trajectory is on the speed constraint. On the singular-γ arc, the costate variables λ_v and λ_ψ are obtained by integrating (13)-(15) instead of finding them directly from (27) and (28); we find λ_h directly from (24), whereas on the speed constraint λ_h is computed directly from (43). In this relatively simple case of a heading capture with specified altitudes and speeds, the costate variables can be treated as parameters in such a manner that families of extremals will sweep out all desired end conditions. To achieve this, forward time integration must be used for descent and reverse time integration for ascent. For convenience of integration the (x,y) coordinates at the 10,000-ft altitude were chosen (0,0). This technique permits the path integration to be started on a constrained or a singular portion of the path, which limits the freedom of choice for the adjoint variables and makes it easier to pick them from the limited set. When starting on a singular portion of the path, the optimal path leaves the singular arc as required by the end conditions, provided the solution is not forced off by failing to meet the speed constraint or the generalized Legendre-Clebsch condition (eq. (39)). When starting on a speed-constrained portion of the path, the optimal solution will leave the constraint boundary as required by the end conditions, provided the solution is not forced off by failing to meet $\eta > 0$. If in the singular-γ-arc descent, the speed constraint is violated before reaching the reference altitude of 2000 ft, the guidance switches to the speed-constrained arc at this point. The singular-γ case and the speed-limited case are discussed separately.

The Singular-γ Case

As previously discussed, λ_v and λ_ψ can be obtained from (27) and (28) and λ_h from (24). With the thrust $T = T_{max}$ or $T = T_{min}$ and h given (h = 10,000 ft), the only remaining variable of choice is v. In addition, λ_ψ must be close to but not equal to zero for turning to occur in the lower-altitude portion of the flightpath with almost a straight-line flight in the higher-altitude portion. Therefore, we choose v iteratively to solve (31), which is the condition for $\lambda_\psi = 0$ in (28). Small variation from the speed thus found will permit us to generate extremals which cover the range of heading $0 < \psi < 180°$. Changes in v to cover the range of headings were so slight (in the order of 10^{-19} knots) that double-precision calculations were required. For all extremals, the generalized Legendre-Clebsch condition (39) remained valid over the range of altitudes considered. For practical purposes, we determined v from (31), λ_v from (30a) or (30b), and selected λ_ψ over a small range to cover all turns (0 - 180°).

Based on the constraint for flightpath angle, $\gamma_{max} = 0°$ in descent and $\gamma_{min} = 0°$ in climb, an initial descent in the optimal climb trajectories or a final climb in the descent trajectories are not allowed, even though they may have lower cost. If in the singular-γ-arc descent the speed constraint is violated before reaching the reference altitude of 2000 ft, the guidance must switch to the speed-constrained arc. In most cases, getting off the singular-γ-arc or the speed-constrained arc at the lower reference altitude h = 2000 ft transfers the path to the zero degree glide slope angle and maintains it there while turning and reducing the speed to 180 knots. For optimal descent with large turn angles, the optimality condition (23) demands a step change of glide slope angle which brings the extremal to an incorrect final altitude. By getting off the singular-γ arc at a higher altitude, the proper final altitude at the proper speed could be obtained after a few iterations. Whatever final heading is obtained, the resulting extremal provides one example of an optimal heading change climbout or descent maneuver. A second method to force a flat turn after leaving the singular arc consists of constraining the permissible γ to a narrow range.

The Speed-Limited Case

If λ_v is treated as a parameter, λ_h is determined via (43); λ_ψ can be obtained by solving equation (12) and replacing λ_h with equation (43), u with equation (21) for an unsaturated bank angle, and γ with equation (40).

$$\lambda_\psi = \pm 2v\sqrt{-[C_0 + C_1T + C_2T^2 + Cv - \lambda_v g(T - D_1)/W]\lambda_v D_2/(gW)} \tag{46}$$

Again, the choice of one adjoint variable determines the other two once the thrust is chosen (T = 0 or $T = T_{max}$). As before, initially u, and hence λ_ψ, must be extremely close to zero. Hence, from (46) λ_v must be close to

$$\lambda_v\Big|_{\lambda_{\psi=0}} = -(C_0 + C_1T + C_2T^2 - Cv)W/[g(T - D_1)] \tag{47}$$

Now from (18) and (20), λ_v must be in the range

$$-WC_1/g \le \lambda_v \le 0 \quad \text{for} \quad T = 0 \tag{48}$$

and from (18)

$$\lambda_v \leq -(C_1 + 2C_2T_{max})W/g \quad \text{for} \quad T = T_{max} \tag{49}$$

The above considerations limit the possible values of λ_v that can be considered when starting on the speed constraint. In addition, η in (45) must be positive, so that an extremal on the constraint can be considered a candidate for an optimal flightpath.

We remember that C in (47) is the cruising efficiency: pounds of fuel per foot traveled at the cruising speed. The number depends in a minor sense on the stage length. Or, for $C = 0$ in the performance criterion, we would obtain the minimum fuel climbing or descending heading capture flightpath, which does not consider any continuation of the path. Therefore, the permissible range of λ_v shall be translated into the equivalent range for C. For descent, $T = 0$, the two limits in (48) for λ_v are used and solved in (47) for C. This gives

$$(C_0 + C_1D_1)/v \geq -C \geq C_0/v$$

numerically

$$0.00407 \geq -C \geq 0.000148$$

The equation for $\eta(0)$, (45), is a linear function of C and must be positive. Numerically, $\eta(0)$ just passes through zero as C becomes greater than -0.00237. Hence, C must be in the range

$$0.00237 \geq C \geq 0.000148$$

Hence both C's that are considered ($C = 0$ and $C = 0.00288$ lb/ft = 17.5 lb/n. mi.) are outside the allowable range. It is therefore concluded that descent on a 250-knot speed bound is not optimal. This conclusion will be confirmed by results for the singular-γ arc where it has already been shown that the speed of descent on the singular arc is below the speed constraint of 250 knots. Similar considerations for the climbout show that extremals calculated for both C's are candidates for optimal flightpaths. Again, small variations from the value given in (47) will cover all possible heading changes (0 - 180°) and as in the singular-γ case the sign ambiguity for λ_ψ (46) provides for right and left turns.

RESULTS

We will first discuss the special case for straight-line ascent and descent ($\Delta\psi = 0$) to tie our data with that of (1). This will be followed with results for optimal turning ascents and descents.

Figure 2 is a plot of the altitude-versus-speed profiles for straight-line climb and descent. The thin lines are a reproduction of a figure from (1) for a 200-n. mi. altitude-speed profile, which we will use for verification of our results. The singular-γ-arc ascent profile, denoted by '1' in figure 2, is above the FAA terminal-area speed constraint. The altitude-versus-speed profile connects to the profile for the complete 200-n. mi. path (point A) at a speed somewhat less than the speed at which the ascent is resumed from the 10,000-ft altitude (point B). This is a result

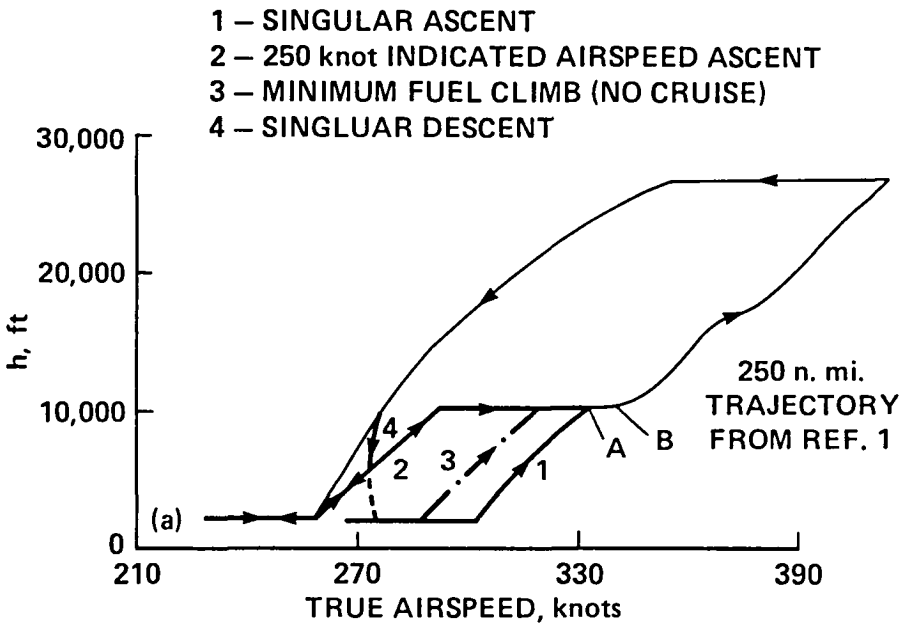

(a) Altitude-speed profile.

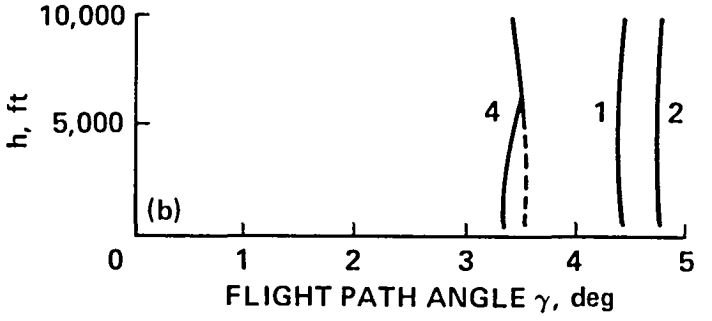

(b) Flightpath angle command.

Figure 2.- Straight-line optimal flightpaths.

of a conservatively chosen T_{max} of 23,000 lb. By setting T_{max} at 25,000 lb the 10,000-ft intercept shifts to 338.5 knots, indicating that the following climb is the continuation of the singular-γ arc. It is thought that this is closer to the effective T_{max} used in (1). As discussed before, the FAA often permits a climbout faster than 250 knots IAS. In this case, the optimal (singular-γ-arc) climbout saves 36 lb of fuel for the total path compared with the speed-limited climbout, denoted by '2' in figure 2, which is followed by an acceleration to the singular-γ-arc speed at the 10,000-ft altitude. Figure 2 also shows (dash-dot line '3') the singular-γ-arc climb for $C = 0$, which would be the optimum climb profile if the cruise did not have to be considered. Since an acceleration to the speed at point B (fig. 2) is required, the total cost is higher than for the singular-γ-arc climb with the proper C, but less than the cost for the speed-limited climb.

The singular-γ-arc optimal descent speed, denoted by '4' in figure 2(a), is below the speed limit of 250 knots IAS, denoted by '2' in figure 2(a) and turns more sharply toward the speed constraint than the altitude-speed profile given in (1). Therefore, it approaches the speed constraint at a higher altitude than the example of (1). The altitude-speed profiles are very sensitive with respect to small differences in the engine-idle fuel flow model. For instance, when the modeled engine-idle flow is reduced to one-third of the present value, the singular-γ descent altitude-speed profile will always remain below the 250-knot indicated airspeed constraint. Once the model is fixed, the resulting fuel consumption is not very sensitive with respect to the altitude-speed profile. For instance, flying the mixed descent or a pure singular-γ-arc descent (dashed-line extension of '4') makes less than a pound difference in fuel for the straight-line or even turning descent. Figure 2(b) also shows that for both climb and descent, the γ's remain almost constant, which makes flying these flightpaths relatively easy. With our results for straight-line ascent and descent agreeing well with those of reference 1, we shall first look at the data for turning-ascending flight and then at those for turning descents.

Solutions to the optimization problem that include ascending turns result in altitude-speed profiles that are almost identical to the straight-line optimization problem (see fig. 3(a)), with most of the turn occurring in level flight before ascent from the minimum maneuvering altitude (2000 ft in this example; see fig. 3(b)). To further illustrate the above statement, table 1 summarizes the numerical values for the key flightpath variables as a function of the total heading change for both singular-arc and speed-constrained ascents. We notice from table 1 that the speed at which ascent begins (column 3) depends on the type of ascent and not on the required total heading change (column 2). A similar statement is largely true for the initial

TABLE 1.- NUMERICAL VALUES OF KEY FLIGHTPATH VARIABLES IMMEDIATELY AFTER SWITCH-OVER FROM LEVEL TURN TO CLIMB

Case (1)	ψ_{total}, deg (2)	v, knots (3)	γ at h = 2000 ft, deg (4)	$\Delta\psi$ to go, deg (5)	ϕ, deg (6)	Type of ascent
I	0	301.7	4.356	0	0	Singular arc
II	90	301.7	4.355	1.6	1.7	Singular arc
III	180	301.7	4.353	5.2	5.2	Singular arc
IV	0	258.1	4.79	0	0	Speed constrained
V	90	258.1	4.76	9.2	7.2	Speed constrained
VI	180	258.1	4.65	30	17.8	Speed constrained

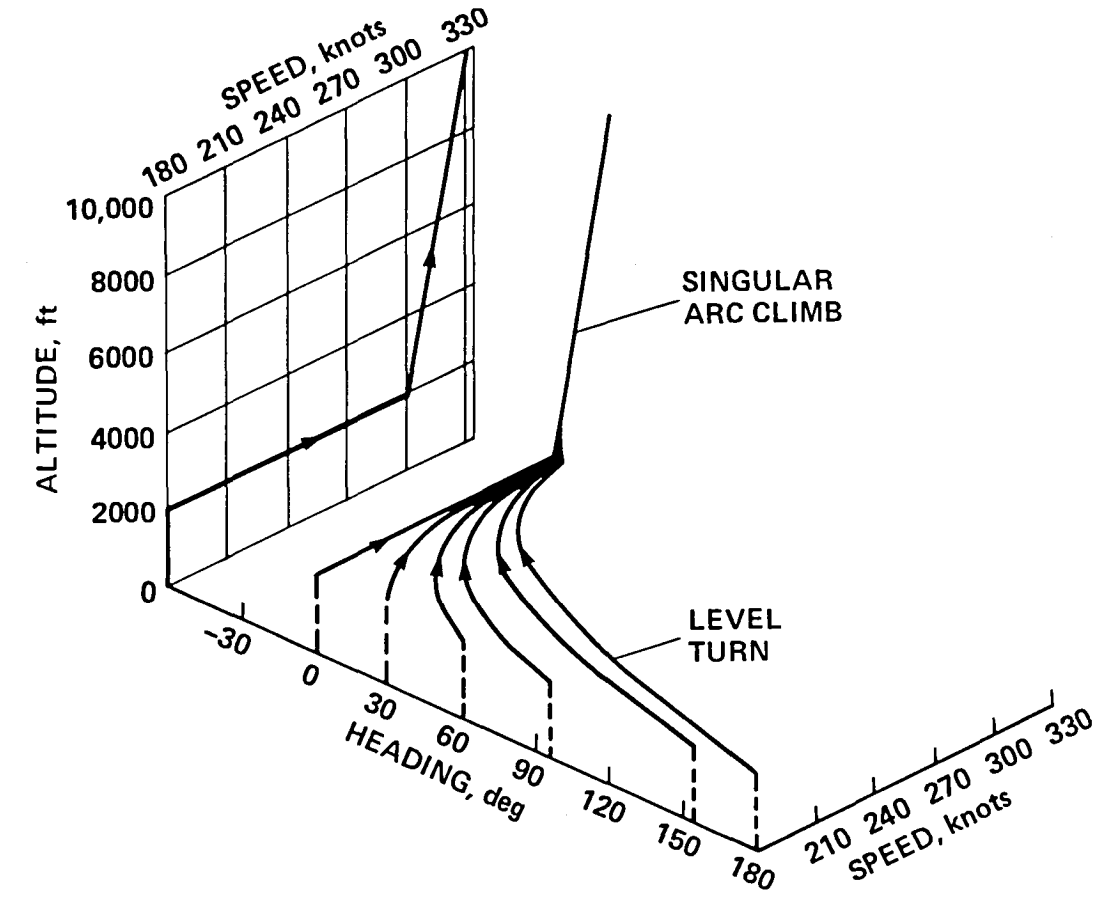

(a) Field of extremals.

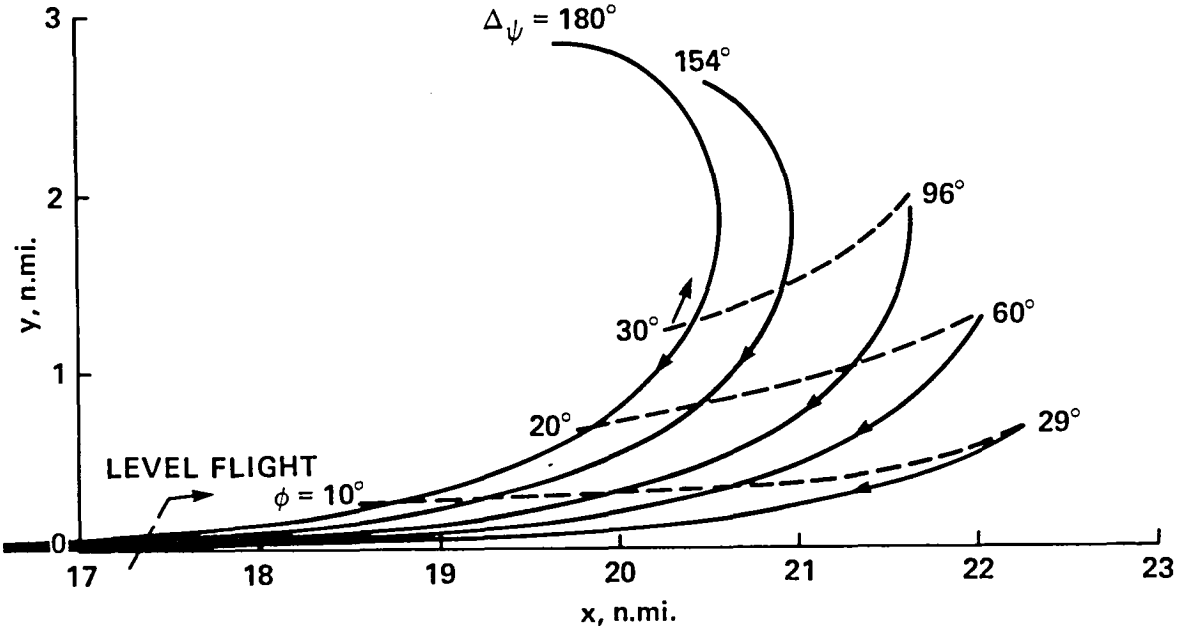

(b) Horizontal projection.

Figure 3.- Optimum turning climbout on the singular-γ arc.

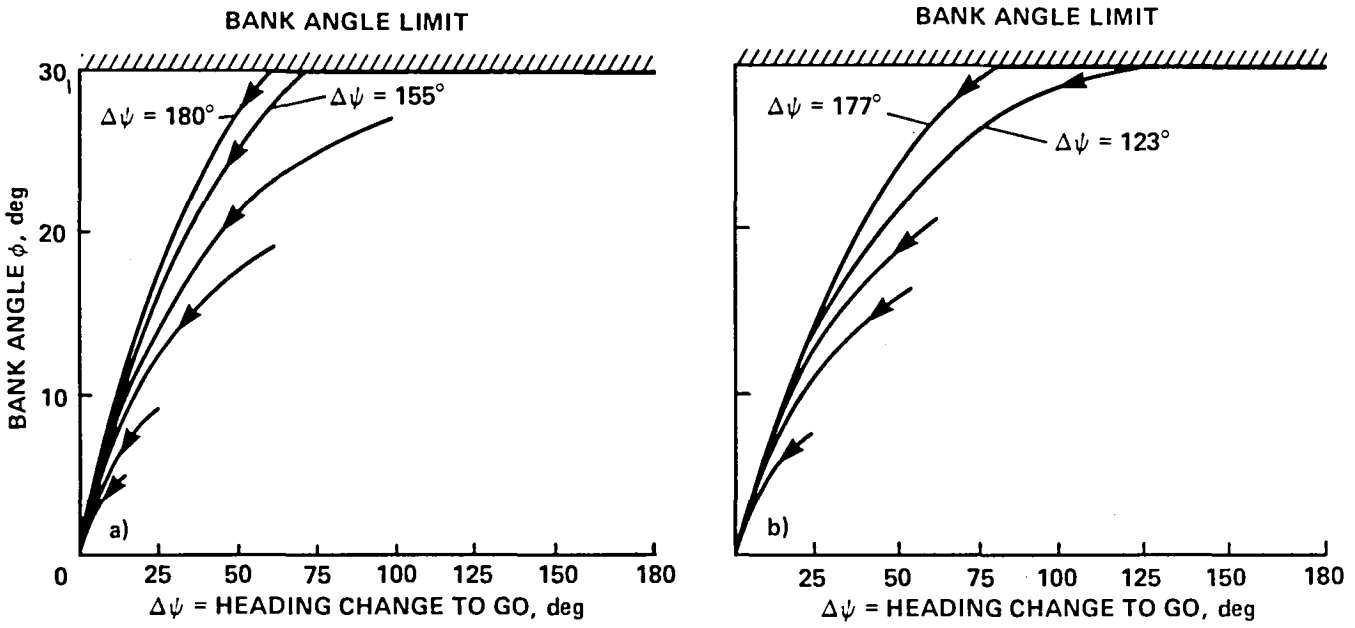

Figure 4.- Bank angle versus heading-change-to-go in optimal climbout. $\Delta\psi_m$ = maximum heading change.

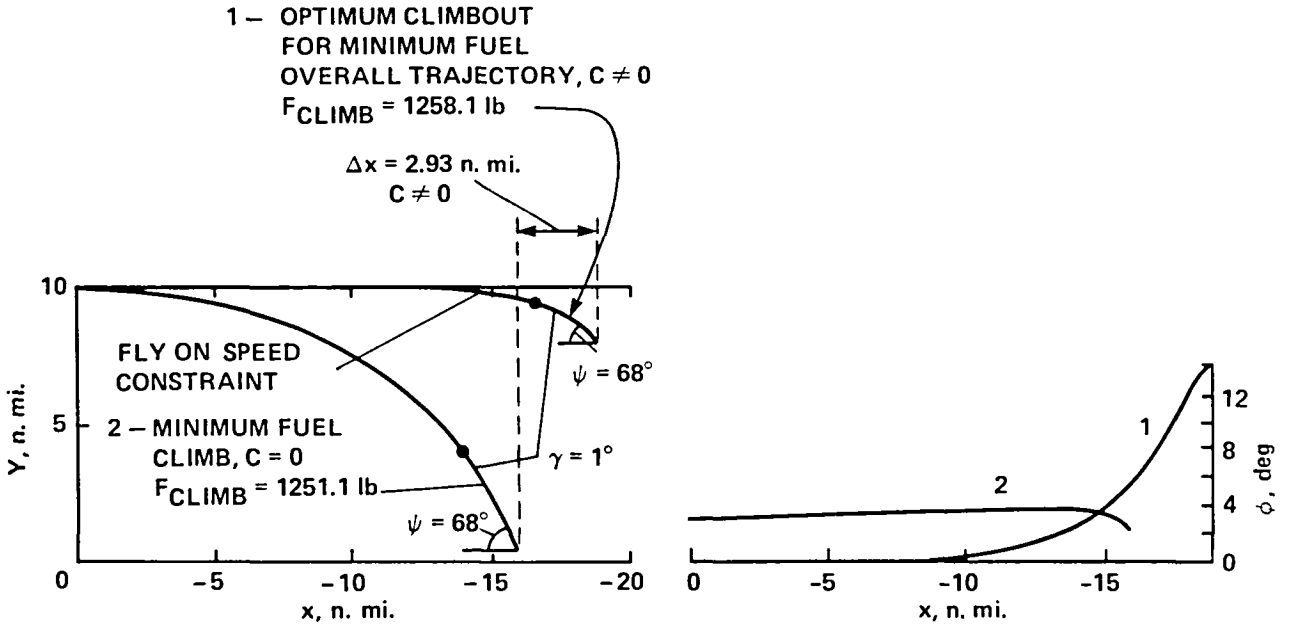

(a) Horizontal projection.

(b) Bank-angle histories.

Figure 5.- Comparison of two types of optimal climbouts.

flightpath angles, which vary only minimally (column 4). The bank angles experienced during the entire turning singular arc and speed-constrained climbouts are shown as functions of the heading change in figures 4(a) and 4(b), respectively. We notice that the bank angles gradually go to zero as the desired heading ($\Delta\psi = 0$) is approached. As table 1 shows for our example (case III), the bank angle at the point of switching from level flight to climb is already as small as 5.2°, indicating that the ascent is almost a straight line. Also, for a turn of more than 90°, the early part of the turn is flown nearly at or at the bank-angle saturation. Intuitively this makes sense, because while flying away from the target we must turn as fast as possible. (This is true in spite of the opposite effect that maximum bank angle has on acceleration, which also must be maximized.) The penalty of observing the speed constraint is about 36 lb of fuel, independent of the amount of turn.

The altitude-speed profile for the singular-γ-arc climb (fig. 3(a)), can be well approximated by a constant IAS speed climb. If we set the speed constraint to a value that corresponds to the singular-arc speed at 10,000-ft altitude — 331.4 knots — the resulting performance is basically identical with the singular-γ-arc performance.

In figure 5 we compare the minimum fuel climb, which considers the fuel saved by flying a shorter cruise distance with the equivalent minimum fuel climb ($C = 0$) for a heading change of 68°. The latter indeed takes 7 lb less fuel, but it climbs in an x-distance that is 2.93 n. mi. shorter, thus requiring an additional 52 lb of fuel for the longer cruise. The bank-angle histories, shown in figure 5(b), are quite different for the two cases.

For the optimum descent only an extremal starting with a singular-γ-arc descent is a candidate for optimality (fig. 6(a)). We note here that this turning descent has actually three phases: singular arc, constant indicated airspeed arc, and level deceleration. Again, most of the turn occurs in level flight (fig. 6(b)) and the altitude-speed profiles are identical within the power of resolution of the graph (fig. 6(a)). Figure 7 shows the bank angles versus heading. The bank angles essentially follow the same curve independent of the total heading change. This allows a simple approximation of the optimal descent in an onboard algorithm. Note that for this example the beginning of the turn is executed with gradually increasing bank angle until, for heading changes greater than 25°, the bank angle is at its maximum. For turns greater than 90° this is required to turn as fast as possible with as large a deceleration as possible to the final speed and heading. The performance index increases with the turn angle, since only the x-distance flown reduces the en route portion of the flightpath. However, the fuel for the final descent decreases slightly for larger turn angles, since the increased bank angle increases drag, which brings the aircraft more quickly to the desired final speed.

Table 2 summarizes the numerical values for the key flightpath variables as functions of the total heading change, ψ_T. The entries in table 2 are similar to those in table 1, except for the addition of column 3, which indicates the altitude at which the system leaves the singular-γ arc. The situation for descent is somewhat more complex than for the ascent; this will be explained by means of the six representative cases in table 2. For small turn angles (see cases I and II, table 2), the singular-γ descent to 2000 ft is followed by a horizontal decelerating turn.

As stated earlier, for large angles of turn the optimal path required a change in γ from γ_{max} (level flight) to γ_{min} part way in the final turn, after having left the singular-γ arc (see cases III and IV, table 2). The changes in altitudes for γ-switching that are required would make an onboard algorithm quite complex. Therefore, the following test was made. Upon leaving the singular-γ arc we forced

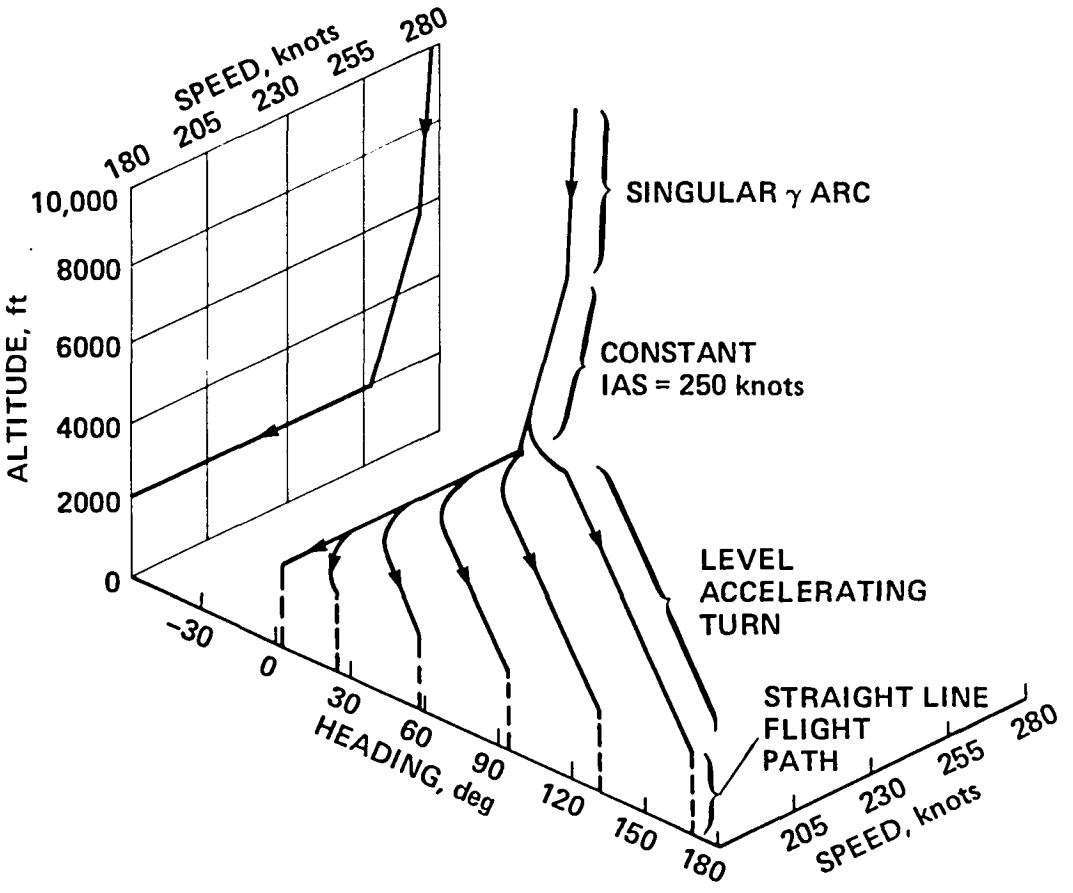

(a) Field of extremals and v - h diagram.

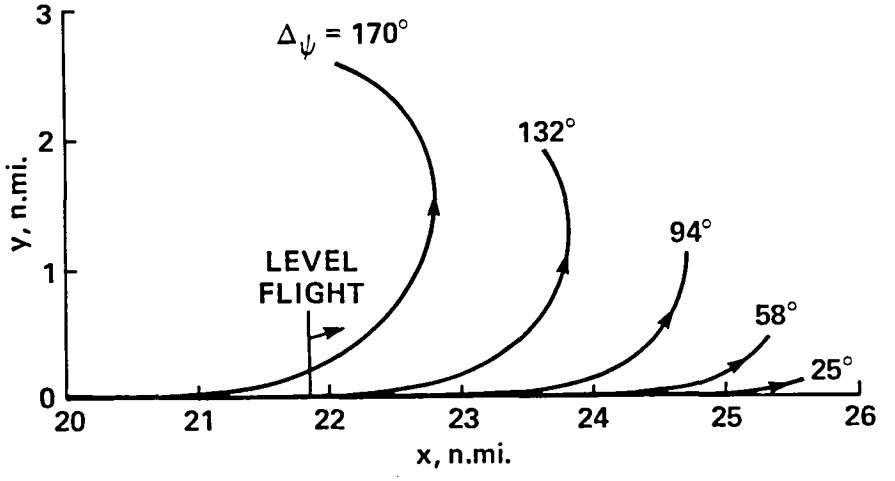

(b) x - y plot of the turns.

Figure 6.- Optimum turning descent with forced level turn.

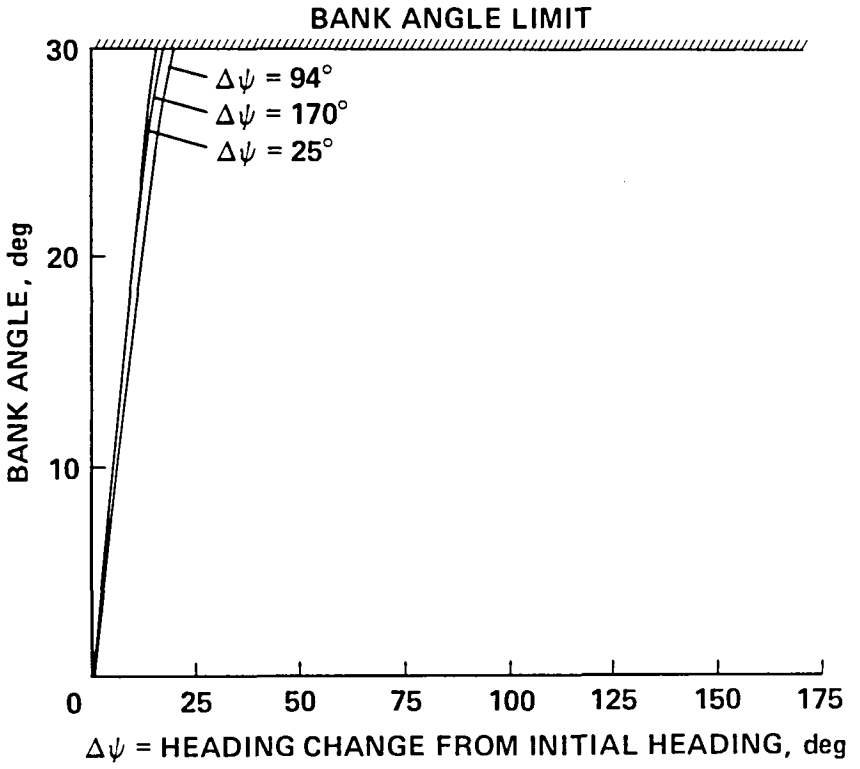

Figure 7.- Bank angles for singular-γ-arc descent.

TABLE 2.- NUMERICAL VALUES OF KEY FLIGHTPATH VARIABLES IMMEDIATELY BEFORE SWITCH-OVER TO LEVEL TURN

Case (1)	ψ_T, deg (2)	h switch to level turn (3)	V, knots (4)	γ_{SA}, deg (5)	$\Delta\psi$ during descent, deg (6)	ϕ, deg (7)	Comments
I	0.4	2000	258.6	-3.35	0.0	0.0	$\gamma_{max} = 0°$, $\gamma_{min} = 4°$
II	58.1	2000	258.6	-3.35	0.0	.02	System wants to stay at γ_{max}
III	109	2025	259.1	-3.28	3.6	3.6	$\gamma_{max} = 0°$, $\gamma_{min} = -4°$
IV	166	2591	257.1	-3.28	4.6	4.6	System switches to γ_{min} after initial level turn
V	132	2000	258.6	-3.35	1.3	2.3	$\gamma_{max} = 0°$, $\gamma_{min} = -0.001°$
VI	170	2000	258.1	-3.78	20.0	30.0	System forced to level turn

the aircraft to stay at 2000 ft by setting very narrow limits for maximum and minimum γ (see cases V and VI of table 2). We find that there is a negligible difference between performances for the optimal case with the γ-switching and the corresponding constant-altitude decelerating turn. Beyond $\Delta\psi = 170°$ a bank angle of 30° (u_{max}) is reached on the singular arc, which switches to a positive γ_{SA} for a quick decelerating turn. Since $\gamma_{max} = 0°$ is violated, we must get off the singular-γ arc as soon as u_{max} is reached. However, for purposes of a possible onboard algorithm, we studied a 180° turn singular-γ descent such that when u_{max} is reached before the 2000-ft altitude, we then continue nonoptimally at constant $\gamma_{min} = -4°$ to 2000 ft, followed by $\gamma_{max} = 0°$ such that $V_{final} = 180$ knots is reached at the completion of the turn. Again, there is only a 3.2 lb of fuel increase for this case compared to the optimal case.

To summarize, for a simple descent, which involves a final level turn, the altitude-speed profile deviates only slightly from the straight-line flight even for the largest heading change (column 4 of table 2). Similar to the ascent, most of the turn is accomplished in level flight ($\psi_T - \Delta\psi$ of columns 2 and 6 of table 2).

The question of global optimality remains. We must find all extremal controls and choose one with the lowest cost. We have shown earlier that on the singular-γ arc and on the speed limit we have single-parameter families of extremals. The variations of those parameters were very small in order to cover the range of final headings. For larger changes we get descending or ascending turns that include a 360° loop. Since our object is to cover large distances in the x-direction, such large turns will not be optimal. Also, from the problem formulation, turns above 180° will not be optimal, since they could be replaced by smaller turns in the opposite direction without increasing the cruise cost, and the cost of the turn always increases with the magnitude of the heading change. We are aware, however, that we have not studied extremals that do not include either a singular arc or a speed-limited section. Therefore, while we have not proved this, we have reason to suspect that our flightpaths are indeed globally optimal.

COMPARISON OF OPTIMAL PROCEDURES WITH VARIOUS SUBOPTIMAL PROCEDURES

The question is often asked how much fuel is saved by using the optimal procedure. Such questions are difficult to answer, since we must ask: "What should the optimal procedure be compared with?" We shall compare reasonable suboptimal climbout procedures which more and more closely mimic the optimal. First let us assume that the optimal climbout altitude-speed profile for straight-line flight is known, and that we will fly at least the latter part at an approximation of the optimal altitude-speed profile. Such an approximation is a climb at maximum thrust at a flightpath angle, which is the average of the singular gamma angle. This assures us that we will meet the terminal conditions. In addition, for all climbout procedures starting at 2000-ft altitude we shall execute an initial maximum bank-angle turn until the desired heading is reached and continue with straight-line flight. The only variations in the climbout procedure considered are the initial climb angles until the singular-γ speed is achieved.

The results are shown in figure 8. Let us first consider an initial 3° climb. The additional fuel is between 10 and 28% over the optimum, which is 285 lb of additional fuel for a 180° turn. If we climb at a slower rate of 500 ft/min, the extra fuel cost is about 4% or 36 lb for the 180° turn. The best approximation of an optimal turning climbout is an initial horizontal flight. Here the additional cost is primarily due to the incorrect bank-angle schedule. The smallest additional cost beyond the optimal is due to flying a constant γ as an approximation of the slightly varying singular γ. This is illustrated in figure 9, where we plot the additional fuel when we change the climb angle from the average singular γ. Over a range of 0.04° the cost deviates from the optimal by only 0.1 lb, and it is fairly insensitive for errors of ±0.15° from the singular γ. Considering these results, we can say that the most important fuel-saving feature of the optimal climbout is the initial horizontal turn and acceleration up to the singular-γ speed. In fact, if an initial dive would have been permitted, more fuel could have been saved.

We can make a similar investigation for the turning descents. Again, we descend on a flightpath angle, which is the average singular-arc descent angle. At a certain altitude we reach a speed of 250-knots indicated airspeed. At this point we select the varying flightpath angle which will hold this airspeed. When we reach the desired altitude, we go to the final flightpath angle, which is nominally 0°, and begin the turn at maximum bank angle in such a manner that the desired heading and final speed are reached simultaneously.

It should be noticed for the following that the optimal flightpaths with which we are making the comparison are constrained to a level final turn. We stated earlier that for large turns, where the maximum γ was constrained to 0° and the minimum to -4°, it was optimal to begin the level turn at a higher altitude than the final altitude and finish the turn at -4° to end up at the desired final altitude and speed.

We compare the constrained optimal descent with various suboptimal ones, where the only change is the flightpath angle of the final turn (see fig. 10). For the descent that mimics the optimal descent most closely (final flightpath angle = 0°), the suboptimal performance is within 0.2% for all heading changes. Again, a final descending turn will usually result in an increase of fuel used. For large turns this trend reverses, since this approximates better the less constrained final optimal turn. If we permit a final climb (and the initial undershoot in altitude, which is

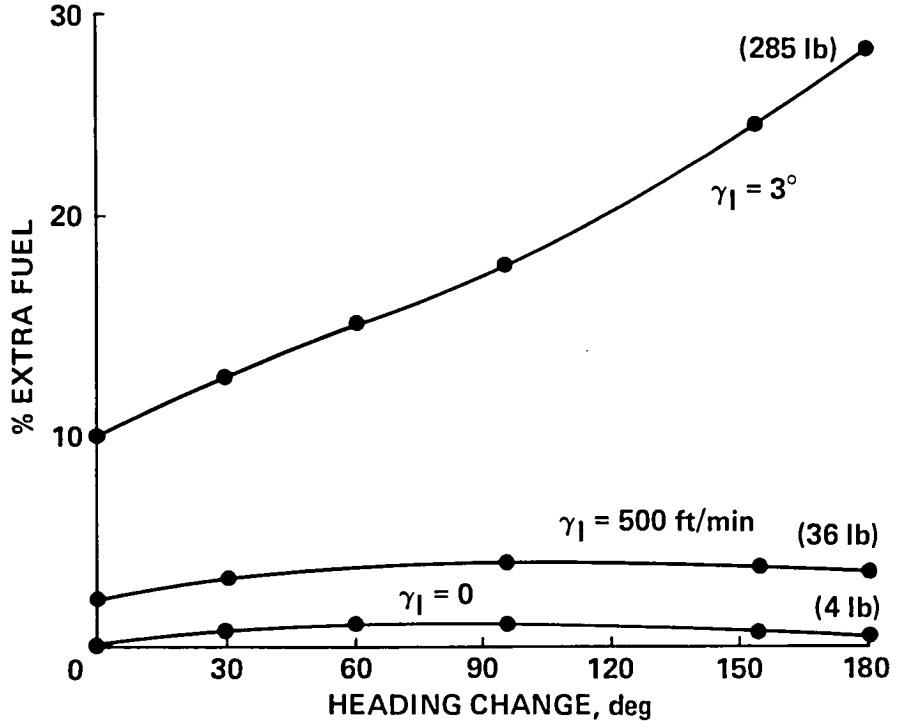

Figure 8.- Extra fuel expenditure for various suboptimal climbout strategies.

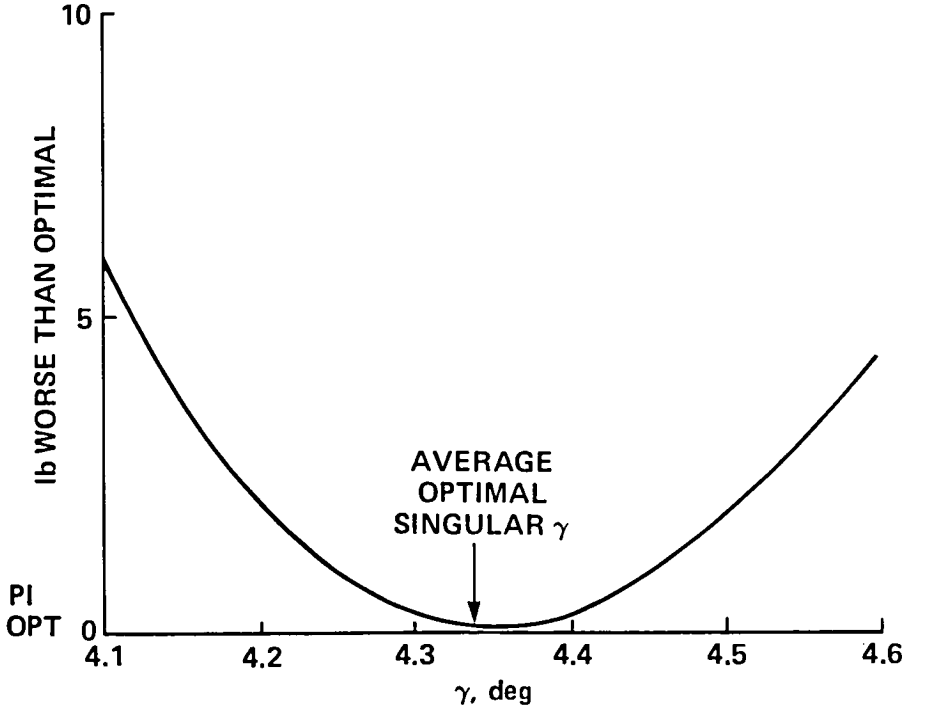

Figure 9.- Change in climbout fuel cost for various climbout angles.

connected with it) for small angles of turn, the suboptimal descent performs slightly better than the optimal, which was constrained not to climb during the descent. Since descent is executed with idle thrust, the above changes in performance are not as significant in terms of fuel as the changes from the optimal for the turning climbout.

CONCLUSIONS

1. For onboard optimization of fuel-efficient turning descents and climbouts, it is sufficient to use an existing climb-cruise-descent fuel-optimization algorithm and superimpose initial- and final-level turns from and to the airport.

2. Relaxation of the speed limit for climbout of the 727-100 can save 36 lb of fuel per climbout, independent of the required heading change.

3. A constant-IAS climb after an initial-level turn using the optimal bank-angle schedule is a close approximation to the optimal turning climbout.

4. An initial-level accelerating turn to the proper speed before climbing is the most fuel-saving feature in an optimal climbout.

5. The optimal descent starts below the FAA terminal-area speed constraint of 250 knots IAS, then reaches the speed constraint and finally terminates in a decelerating level turn.

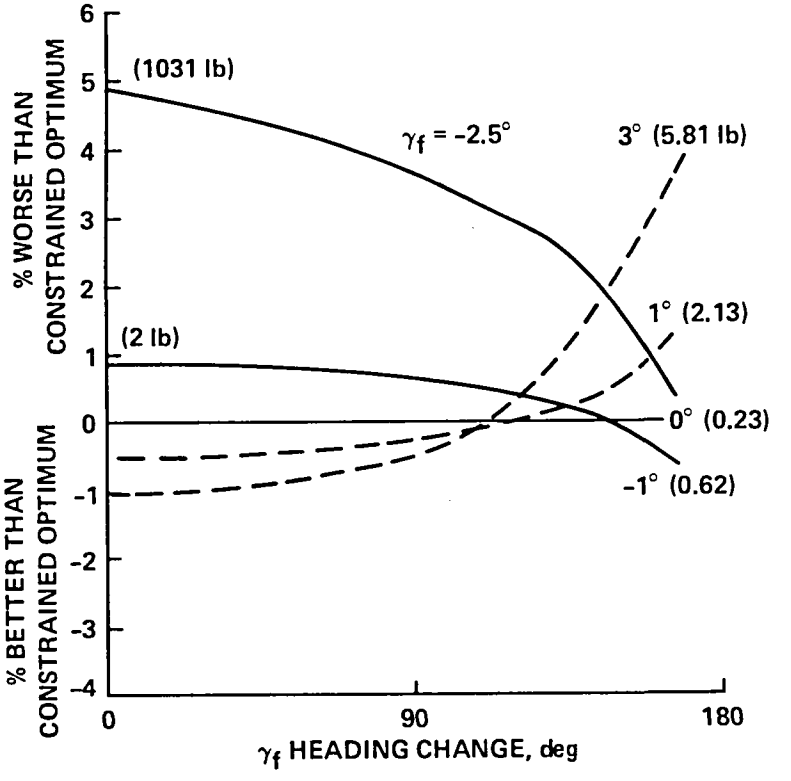

Figure 10.- Optimal versus suboptimal descents.

APPENDIX A

The Drag and Fuel Flow Equations

Reference 1 includes subroutines that calculate drag thrust and fuel flow from comprehensive table lookup data over the complete operating range of the Boeing 727-100 aircraft. For our method of calculating extremals, we need functional relationships for the limited range of 150- to 350-knot speeds and 0- to 10,000-ft altitudes, which are derived here.

Drag $D(v,h)$

Over the range of speeds considered, flaps must be deployed for the lower speeds. However, we do not want to consider flaps as a control variable. Therefore, flaps are eliminated by putting a limit on the angle of attack

$$\alpha \leq \alpha_{max} = 8^\circ \tag{A1}$$

and by automatically deploying the minimum amount of flaps so that $\alpha = 8^\circ$ is never exceeded. Although the drag curves are shown for all altitudes, in practice flaps are deployed at low altitudes only. This is in agreement with the optimal results. Since we have the constraint

$$L = W/\cos \phi \tag{A2}$$

the drag is also bank-angle dependent.

$$D = D(v,h,\phi) \tag{A3}$$

It should be noted here that our flap schedule is different from that in reference 1, which deploys flaps as a function of indicated airspeed, as shown in figure A1. Our flap program results show less drag at the lower speeds than the schedule of reference 1. However, neither method represents the real world completely, since, at present, flaps are controlled manually in steps, based on speed cues.

The calculation of the drag proceeds as follows. Given h and v from the 1962 atmospheric model, we obtain density ρ and Mach number, M. Knowing the bank angle, we calculate the required lift coefficient to meet the constraint (A2)

$$C_L = W/(0.5\ \rho S v^2 \cos \phi) \tag{A4}$$

where S = area of the wings = 1560 ft, W = weight of the aircraft = 150,000 lb, and ρ = density of air at the given altitude. Then, for $\alpha = 8^\circ$ the subroutine CLIFT computes the available lift coefficient $C_{L_{av}}(\alpha,h,M,\delta_f)\big|_{\alpha=8^\circ}$. Starting with zero flaps, the flaps are increased in 0.01° steps until

$$C_{L_{av}} \geq C_L \tag{A5}$$

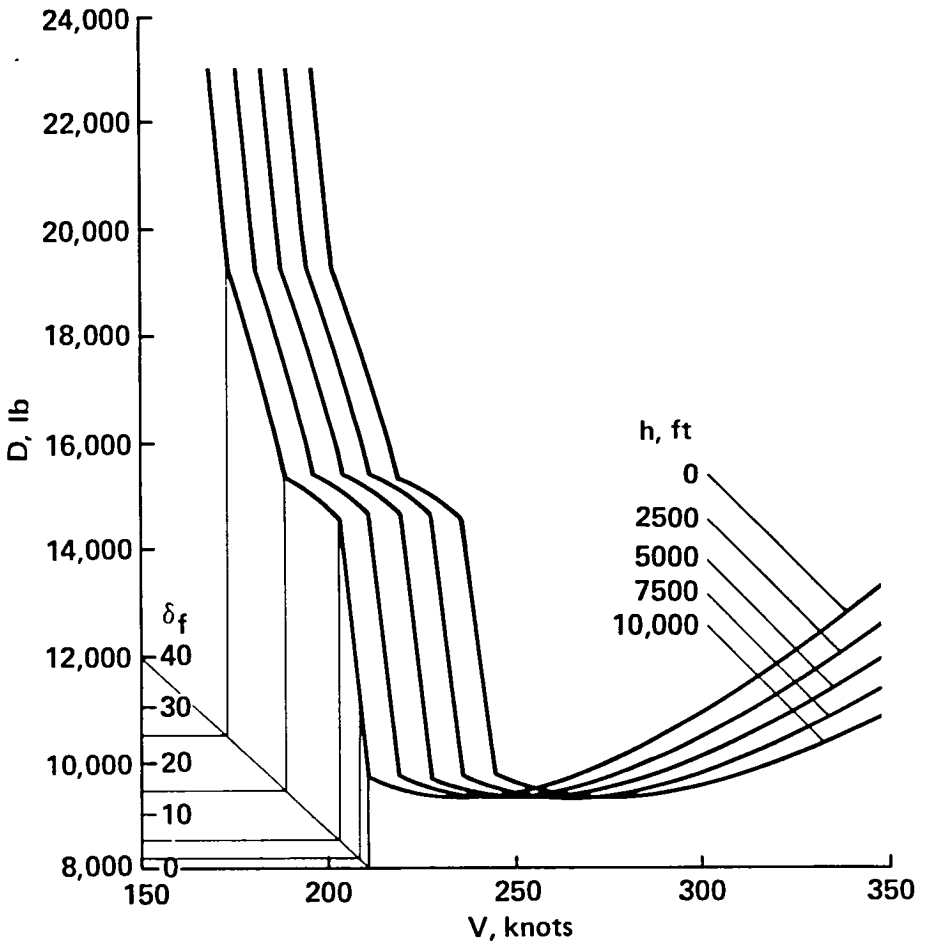

Figure A.1.- Erzberger flap program: $\phi = 0°$.

The final flap value is the value used in the subroutine CDRAG which determines the drag coefficient $C_D(M,C_L,\delta_f)$. This permits us to calculate the drag

$$D = 0.5\ \rho S v^2 C_D = D(h,v,\phi)\big|_{\alpha \le 8°, L=W/\cos\phi} \tag{A6}$$

An example of the drag curves obtained by the above method, including the flaps required, is shown in figure A2. The bumpiness of the drag-versus-speed curves in the region where flaps are deployed is an artifact of linear interpolation of the drag polars which are given only for 0°, 2°, 5°, 15°, 25°, and 40° flap angles. Our model therefore should smooth out these bumps.

Our task is to match the drag data with an analytic expression. In order to minimize the number of parameters required, we shall first develop an expression from the approximate theory of wings, and then determine parameters that fit the data.

The lift coefficient of a clean wing is

$$C_L = C_{L_\alpha}\alpha \tag{A7}$$

Adding flaps shifts the curve upward

$$C_L' = C_{L_0} + C_{L_\alpha}\alpha \tag{A8}$$

Without flaps the lift-drag polar is

$$C_D = C_{D_0} + yC_{L_\alpha}\alpha^2 = C_{D_0} + \eta C_L\alpha \tag{A9}$$

Assuming the same form when the drag polar is shifted due to flaps adds a linear term in α.

$$C_D' = C_{D_0}' + y'C_{L_\alpha}' = C_{D_0}' + \eta'\left(C_{L_\alpha}\alpha + C_{L_\alpha}\alpha^2\right) \tag{A10}$$

From (A4) and (A8) we can solve for

$$\alpha = \left[W/(0.5\ \rho S v^2 \cos\phi) - C_{L_0}\right]/C_{L_\alpha} \tag{A11}$$

and using (A11) to replace α in the drag equation (A10) results in an equation for drag of the form

$$D = C_D'\ 0.5\ \rho S v^2 = k_0/\cos\phi + k_1 v^2 + k_2(1 + \tan^2\phi)/v^2 \tag{A12}$$

where the k's are functions of ρ, S, W, η', C_{L_0}, C_{L_α}, and C_{D_0}'.

This is the form of the functional relationship for a constant altitude and constant flap angle. In actuality the flap changes with speed for constant altitude as shown in figure A2. The bank angle, which is one of the controls, appears twice in the above expression. The first approximation of the k's in (A12), which must be functions of altitude, are found as follows. We write for $\phi = 0$

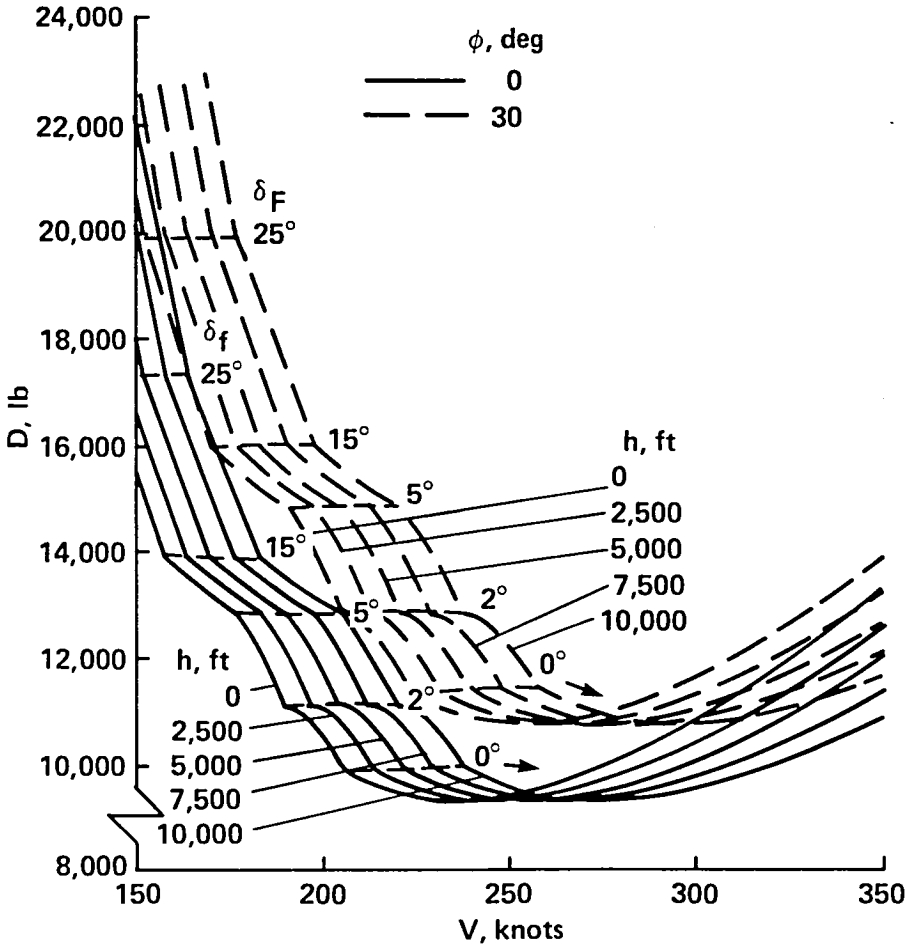

Figure A.2.- Drag versus speed from table lookup.

$$D = k_1(1 + k_2h) + k_3(1 + k_4h)v^2 + k_5(1 + k_6h)/v^2 \quad \text{(A13)}$$

Using the tabular data graphically represented in figure A2, for $h = 0$, and for three different speeds of 150, 225, and 350 knots, we obtain three equations with three unknowns, k_1, k_3, and k_5. With these solved, we chose $h = 10{,}000$ ft and solve for k_2, k_4, and k_6. These six constants are a good first approximation to the drag equation. These constants are then used for the complete drag equation (A12)

$$D = k_1(1 + k_2h)/\cos\,\phi + k_3(1 + k_4h)v^2 + k_5(1 + k_6h)(1 + \tan^2\,\phi)/v^2$$

which using $\cos\,\phi = 1/\sqrt{1 + \tan^2\,\phi} \approx 1/(1 + 0.5\,\tan^2\,\phi)$ is approximated as

$$D = k_1(1+k_2h) + k_3(1+k_4h)v + k_5(1+k_6h)/v^2 + [k_1(1 + k_2h)/2 + k_5(1 + k_6h)/v^2]\tan^2\,\phi \quad \text{(A14)}$$

For the purpose of an analytic approximation of the drag function, we generate 180 samples for all combinations of the following parameters:

$\phi = 0°,\ 10°,\ 20°,\ 30°$

$h = 0,\ 2500,\ 5000,\ 7500,\ 10{,}000$ ft

$V = 150,\ 175,\ 200,\ 225,\ 250,\ 275,\ 300,\ 325,\ 350$ knots

and calculate the rms percent error between the table lookup values and the analytic drag equation, where D is in pounds, h is the altitude in feet, and v the speed in knots. By means of an extremum-finding subroutine (ref. 12) the parameters are adjusted to minimize the rms percent error, which results in an rms error of 2.387%. This apparent error is primarily due to the desirable smoothing of the drag curves in the flap deployment region. The polynomial fit agreed within 0.8% (max) with the drag in the $\delta_f = 0$ region. The values of the coefficients in (A14) are:

$$k_1 = -0.4078\times10^4 \qquad k_3 = 0.1146 \qquad k_5 = 0.3830\times10^9$$

$$k_2 = 0.2429\times10^{-4} \qquad k_4 = -0.2005\times10^{-4} \qquad k_6 = 0.4227\times10^{-4}$$

The resulting drag curves are shown in figure A3, which may be compared to the table lookup data in figure A1.

Fuel flow $f(T,v,h)$

Reference 1 presents fuel flow data in tabular form

$$\dot{f}_n = \dot{f}_n(\text{Mach},T_n,h) \quad \text{(A15)}$$

where

$\dot{f}_n$ is a normalized fuel flow rate

$$\dot{f}_n = \dot{f}_n(T\sqrt{\theta}) \quad \text{(A16)}$$

$\dot{f}$ = fuel flow rate

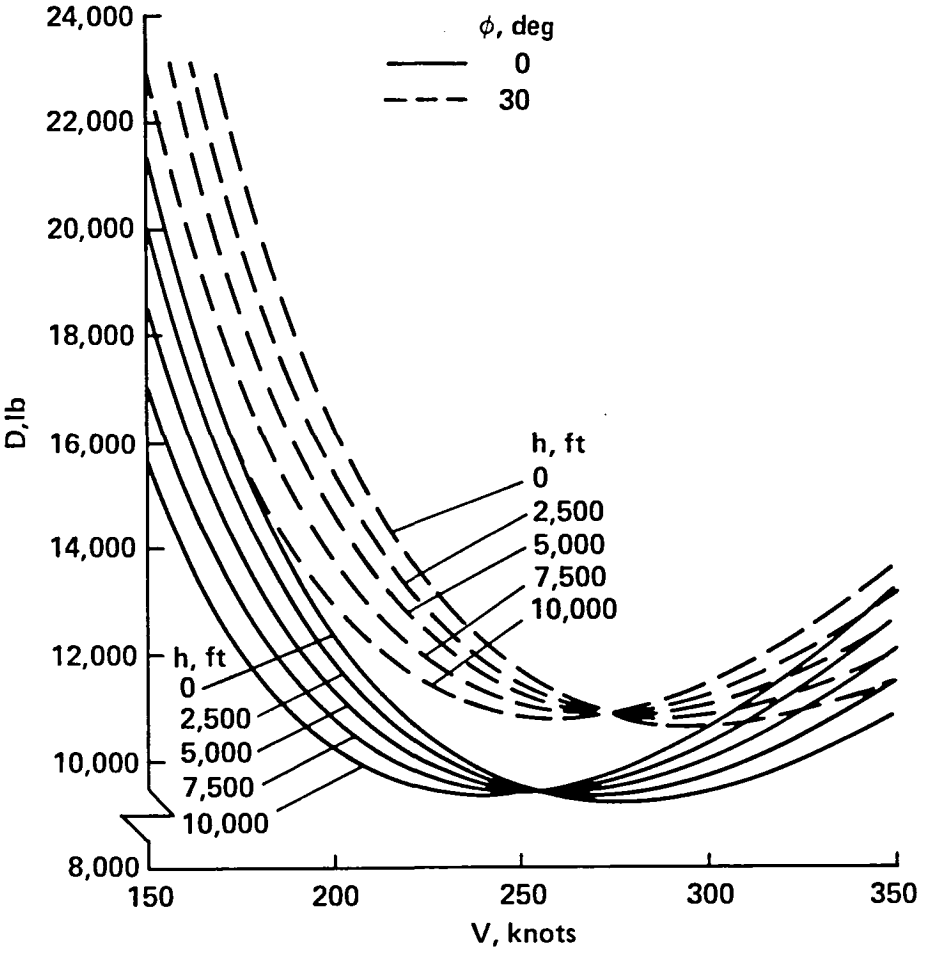

Figure A.3.- Drag versus speed from algebraic equation.

$$T = \text{thrust for three engines} = \delta T_n \tag{A17}$$

where T_n is the normalized thrust for three engines.

$$\sqrt{\theta} = \text{square root of the temperature ratio}$$

$$= \text{temperature at altitude } h/\text{temperature at zero altitude} \tag{A18}$$

$$\delta = \text{pressure ratio} = \text{pressure at altitude } h/\text{pressure at zero altitude} \tag{A19}$$

It is our task, first to determine a functional relationship for fuel flow that involves only T,v,h, second to determine approximate values for the parameters, and third to minimize the error between the analytic representation and the full table lookup of the fuel flow when using the standard 1962 atmosphere.

The $\dot{f}_n$ entries in the three-dimensional table are normalized in such a way that they are almost altitude-independent. For the first two steps of the task we are therefore using only the table for $h = 5000$ ft. In figure A4 the f_n values multiplied by the normalized thrust T_n are plotted over the range of Mach numbers of interest because this quantity is the actual fuel flow normalized by atmospheric constants.

From (A16) and (A17)

$$T_n \dot{f}_n = T_n \dot{f}/(T\sqrt{\theta}) = \dot{f}/(\delta\sqrt{\theta}) \tag{A20}$$

The relationship shown in figure A4 can be approximated as

$$T_n \dot{f}_n = 0.45 + M + \frac{3.75 + 3.35\,M}{30{,}000} T_n + \frac{0.5(1 - M)}{30{,}000^2} T_n^2 \tag{A21}$$

(A20) and (A18) used in (A21) give the actual fuel flow

$$\dot{f} = \delta\sqrt{\theta}\left[0.45 + M + \frac{3.75 + 3.25\,M}{30{,}000}\frac{T}{\delta} + \frac{0.5(1 - M)}{30{,}000^2}\left(\frac{T}{\delta}\right)^2\right] \tag{A22}$$

Fuel flow is still a function of the pressure ratio, temperature ratio, and Mach number, which are all functions of altitude. The altitude dependence for the normal atmosphere is presented in table A1.

TABLE A1.- NORMAL ATMOSPHERE

Altitude $ft\times10^{-3}$	T, K	P, psf	P, $slugs/ft^3\times10^4$	$\delta = P/P_0$	$\sigma = \rho/\rho_0$	$\sigma^{-1/2}$	Sound speed, fps
0	288.15	2116	23.77	1.0000	1.0000	1.0000	1116.9
2	284.19	1968	22.41	.9298	.9428	1.0299	1109.2
4	280.23	1828	21.11	.8637	.8881	1.0611	1101.4
6	276.27	1696	19.87	.8014	.8359	1.0938	1093.6
8	272.31	1572	18.08	.7428	.7860	1.1279	1085.7
10	268.35	1455	17.55	.6877	.7385	1.1637	1077.8

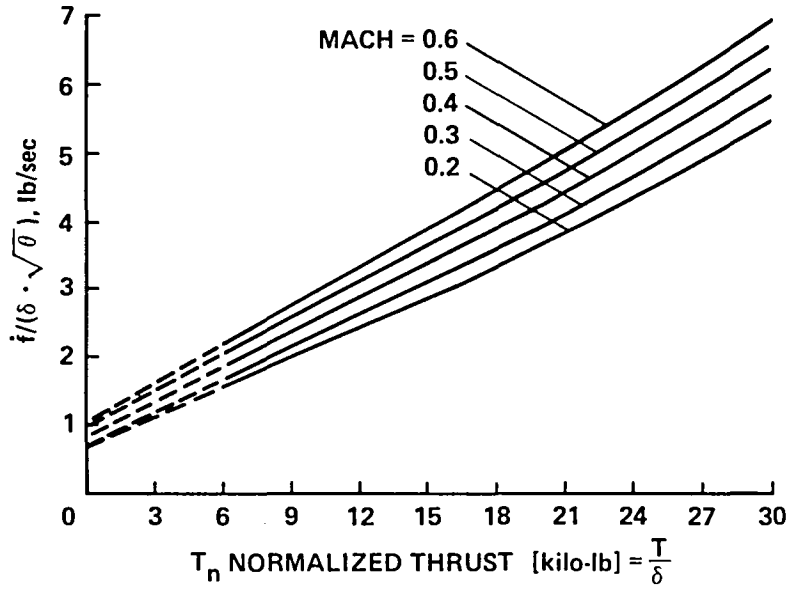

Figure A.4.- Fuel flow rate versus T_n for h = 5000.

We can see from table A1 that the speed of sound decreases with altitude, so that the speed expressed in units of Mach (M) increases with altitude

$$M = v(1 + 0.363\times10^{-5}\ h)/1116.9 \tag{A23}$$

where v is given in feet/second true airspeed. The pressure ratio can be expressed as

$$\delta = 1/(1 + 0.45\ h/10{,}000) \approx 1 - 0.31\ h/10{,}000 \tag{A24}$$

and the square root of the temperature ratio as

$$\sqrt{\theta} = 1 - 0.363\times10^{-5}\ h \tag{A25}$$

Using (A22)-(A25) allows us to obtain $\dot{f}$ when T, h, and v are given. We can rewrite (A22) as

$$f = C_0(h,v) + C_1(h,v)T + C_2(h,v)T^2 \tag{A26}$$

where each of the C's are functions of the atmospheric relations. When (A23) and (A24) are used to replace the atmospheric relations in (A22) and when all higher-order terms except terms involving hv are neglected, all C's end up in the same form:

$$C_j = c_{4j+1}(1 + c_{4j+2}) + c_{4j+3}(1 + c_{4j+4}h)v; \qquad j = 0,1,2 \tag{A27}$$

The numerical values of the twelve parameters in (A27) were used as initial values in the extremum-finding subroutine (ref. 12) where the parameters are adjusted to minimize the rms error between table lookup values for the 200 points given by all combinations of

$$V = 150,\ 200,\ 250,\ 300,\ 350 \text{ knots}$$

$$h = 0,\ 2000,\ 4000,\ 6000,\ 8000,\ 10{,}000 \text{ ft}$$

while using all appropriate fuel flow tables, as well as the exact nominal atmospheric model.

$$T = 7000,\ 9500,\ 12{,}000,\ 14{,}500,\ 17{,}000,\ 22{,}000,\ 24{,}500 \text{ lb}$$

and the values from the analytic expressions (A26) and (A27). This resulted in an rms error of 0.039 lb/sec. The values are:

$c_1 = 0.47537$	$c_5 = 0.10823\times10^{-3}$	$c_9 = 0.91747\times10^{-9}$
$c_2 = -0.24360\times10^{-4}$	$c_6 = -0.80509\times10^{-5}$	$c_{10} = 0.79644\times10^{-4}$
$c_3 = 0.17702\times10^{-2}$	$c_7 = 0.15898\times10^{-6}$	$c_{11} = -0.85521\times10^{-12}$
$c_4 = -0.28995\times10^{-4}$	$c_8 = -0.12439\times10^{-4}$	$c_{12} = -0.45624\times10^{-4}$

For idle thrust

$$c_1 = 0.2528$$

$$c_2 = -0.4\times10^{-4}$$

$$c_3 = 0.147\times10^{-3}$$

$$c_4 = -0.363\times10^{-5}$$

and c_5 through c_{12} are zero. These data are obtained from a table of fuel flow at engine idle. No data are available for an intermediate thrust of 0-7000 lb, which fortunately are not required for this problem. An example of the resulting fuel flow versus thrust function is shown in figure A5.

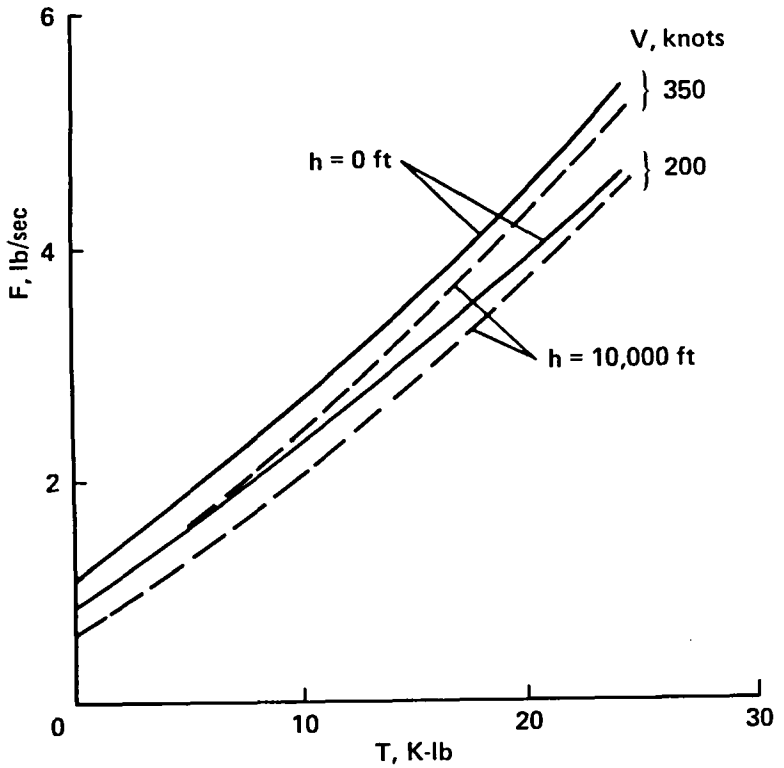

Figure A.5.- Fuel-flow model of the 727-100.

APPENDIX B

In further development we need certain time and other derivations which we shall enumerate here. Let's assume that T = constant and u = time variable.

$$F = [c_1(1 + c_2h) + c_3(1 + c_4h)v] + [c_5(1 + c_6h) + c_7(1 + c_8h)v]T + [c_9(1 + c_{10}h) + c_{11}(1 + c_{12}h)v]T^2 \tag{B1}$$

$$F_v = c_3(1 + c_4h) + c_7(1 + c_8h)T + c_{11}(1 + c_{12}h)T^2 \tag{B2}$$

$$\dot{F}_v = (c_3c_4 + c_7c_8T + c_{11}c_{12}T^2)\dot{h} = F_{vh}\dot{h} \tag{B3}$$

$$F_h = (c_1c_2 + c_3c_4v) + (c_5c_6 + c_7c_8v)T + (c_9c_{10} + c_{11}c_{12}v)T^2 \tag{B4}$$

$$\dot{F}_h = (c_3c_4 + c_7c_8T + c_{11}c_{12}T^2)\dot{v} = F_{vh}\dot{v} \tag{B5}$$

$$D = k_1(1 + k_2h) + k_3(1 + k_4h)v^2 + k_5(1 + k_6h)/v^2 + [k_1(1 + k_2h)/2 + k_5(1 + k_6h)/v^2]u^2 = D_1 + D_2u^2 \tag{B6}$$

$$D_u = 2D_2u \tag{B7}$$

$$D_v = 2k_3(1 + k_4h)v - 2k_5(1 + k_6h)(1 + u^2)/v^3 = D_{1v} + D_{2v}u^2 \tag{B8}$$

$$\dot{D}_v = 2k_3(1 + k_4h)\dot{v} + 2k_3k_4\dot{h}v + 6k_5(1 + k_6h)(1 + u^2)\dot{v}/v^4 - 4k_5(1 + k_6h)u\dot{u}/v^3 - 2k_5k_6\dot{h}(1 + u^2)/v^3 \tag{B9}$$

$$D_h = k_1k_2 + k_3k_4v^2 + k_5k_6/v^2 + (k_1k_2/2 + k_5k_6/v^2)u^2 = D_{1h} + D_{2h}u^2 \tag{B10}$$

$$\dot{D}_h = 2k_3k_4v\dot{v} + (k_1k_2 + 2k_5k_6/v^2)u\dot{u} - 2k_5k_6(1 + u^2)/v^3\dot{v} \tag{B11}$$

$$\dot{D} = D_h\dot{h} + D_u\dot{u} + D_v\dot{v} \tag{B12}$$

$$\dot{u} = u\left[-\left(\frac{1}{v} + \frac{D_{2v}}{D_2}\right)\dot{v} + \frac{\dot{\lambda}_x}{\lambda_x} - \frac{\dot{\lambda}_v}{\lambda_v} - \frac{D_{2h}}{D_2}\dot{h}\right] \quad ; \quad u < u_m \tag{B13}$$

$$\dot{u} = 0 \quad ; \quad u = u_m$$

APPENDIX C

For the minimum principle to apply, the velocity set $(\dot{h},\dot{\psi},\dot{v},F)$ must be convex (refs. 13 and 14). Using equations (3) and (5) for our particular example, figure C1(a) shows that for descent, the velocity set is not convex in the region of zero thrust, due to increased drag at nonzero bank angles. In this case a relaxed (chattering) controller may result in better performance if maximum deceleration will improve performance. To convexize the velocity set we allow the possibility of a chattering bank angle and define a combined control.

$$u = \alpha u_s - (1 - \alpha)u_s = u_s(2\alpha - 1) \tag{C1}$$

where u_s is the magnitude of the tangent of the bank angle $u_s = |\tan \phi|$ and α is the chatter parameter (fig. C1(b)).

α = per unit time the bank angle spends at u_s

$1 - \alpha$ = per unit time the bank angle spends at $-u_s$

then (4) changes to

$$\dot{\psi} = -gu_s(2\alpha - 1)/v \tag{C2}$$

and (12) becomes (assuming $\eta = 0$, off the speed limit)

$$H = F - Cv \cos \psi + \lambda_h v\gamma - \lambda_\psi g u_s(2\alpha - 1)/v + \lambda_v g(T - D_1 - D_2 u_s^2 - W\gamma)/W \tag{C3}$$

Note that the drag is only a function of u_s^2 and does not depend on the value of the chatter parameter α. Now

$$\alpha^* = \begin{cases} 0 & \text{if} \quad \lambda_\psi < 0 \\ 1 & \text{if} \quad \lambda_\psi > 0 \end{cases} \tag{C4}$$

and (20) and (21) become

$$u_s^* = \begin{cases} \nu & \text{if} \quad |\nu| < u_m \quad \text{and} \quad \lambda_v < 0 \\ u_m & \text{if} \quad |\nu| \geq u_m \quad \text{and} \quad \lambda_v < 0 \end{cases} \tag{C5}$$

$$\nu = [(2\alpha - 1)W\lambda_\psi]/[2\lambda_v D_2 v] \tag{C6}$$

We note that when α is nonsingular (49)-(51) give the same result as (21). In this case, (C2) and (C3) revert to the original equations (4) and (12) and we can solve the optimal descent problem as if the original velocity set were convex. However, α is linear and we must consider the singular-α solution.

$$H_\alpha = -2g\lambda_\psi u_s/v = 0 \rightarrow \lambda_\psi = 0 \tag{C7}$$

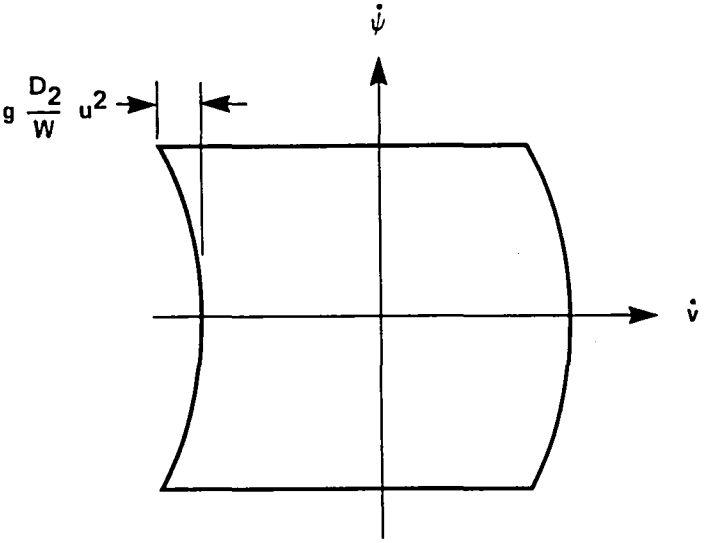

(a) Nonconvex set.

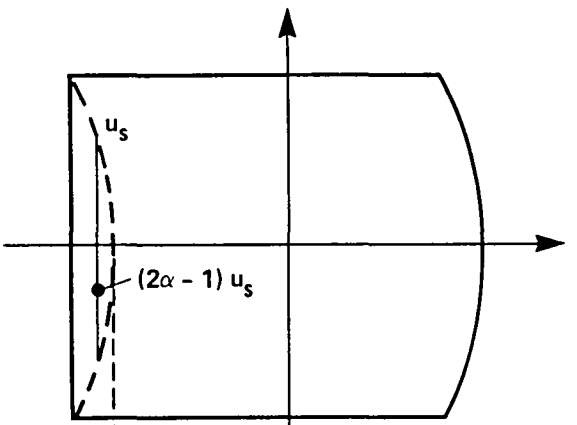

(b) Convexized set which has increased velocity set volume compared to (a).

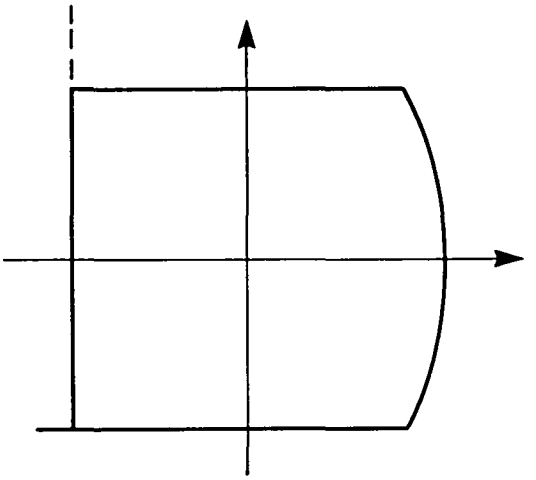

(c) Convexized set which has decreased velocity set volume compared to (a).

Figure C.1.- Cross section through the velocity set $\dot{h}$, $\dot{v}$, $\dot{\psi}$, and F, given v and h.

$$(\dot{H}_\alpha) = 2gCu_s \sin\psi = 0 \rightarrow \psi = 0 \tag{C8}$$

$$(\ddot{H}_\alpha) = -2g^2u_s^2C \cos\psi(2\alpha - 1) = 0 \rightarrow \alpha = 1/2 \tag{C9}$$

$$(-\dddot{H}_\alpha)_\alpha = 4u_s^2g^2C \cos\psi/v \geq 0 \qquad \begin{array}{l}\text{Since } C > 0 \quad \psi = 0 \\ \text{but } \underline{\text{not}} \quad \psi = \pi\end{array} \tag{C10}$$

But from (20) and (C5), $u_s = 0$ when $\lambda_\psi = 0$. This is equivalent to the nonchattering straight descent and again is included in the earlier solutions, which do not require a chattering bank angle.

A different approach to make the velocity set convex is to apply appropriate constraints. This will cut off portions of the earlier velocity set. A reduced velocity set in general means reduced performance. We will therefore reduce the velocity set in such a way as to minimize the excised area. To do this we impose an acceleration constraint, which limits deceleration to a constant value for each (v,h) such that it equals the maximum value which can be obtained at zero bank angle (fig. C1(c)). The resulting deceleration constraint is a mixed state and control constraint

$$\dot{v} \geq -g[D_1(v,h) + W\gamma_{max}]/W \tag{C11}$$

In the following development we only express the changes from the original set of equations, where we express the original equations as before and star (*) the new values. Then from (12) and (C11)

$$H^* = H + \mu\{-g[D_1(v,h) + W\gamma_{max}]/W - \dot{v}\} \tag{C12}$$

Inserting the equation for $\dot{v}$ and simplifying gives

$$H^* = H + \mu\{-g[T - D_2(v,h)u^2 - W(\gamma - \gamma_{max})]/W\} \tag{C13}$$

the adjoint equations (13), (14), and (15) become

$$\dot{\lambda}_h^* = \dot{\lambda}_h - \mu g D_{h_2} u^2/W \tag{C14}$$

$$\dot{\lambda}_\psi^* = \dot{\lambda}_\psi \tag{C15}$$

$$\dot{\lambda}_v^* = \dot{\lambda}_v - \mu g D_{v_2} u^2/W \tag{C16}$$

On the deceleration bound we have $T - D_2(v,h)u^2 - W(\gamma - \gamma_{max}) = 0$ such that

$$\gamma = \gamma_{max} - D_2u^2/W + T/W \tag{C17}$$

We are interested in the decelerating descent at $T = 0$, then γ is just decreased sufficiently to compensate for the additional drag D_2u^2 due to a nonzero bank angle. From $H_\gamma^* = 0 = H_\gamma + \mu g$ we have

$$\mu = \begin{cases} \lambda_v - \lambda_h v/g > 0 & \text{on the deceleration constraint} \\ 0 & \text{off the deceleration constraint} \end{cases} \tag{C18}$$

The >0 requirement for μ on the acceleration constraint is a necessary condition for optimality. Thrust control

$$H_T^* = H_T - \mu g/W$$

Hence the only change from (17) is

$$\tau = -[C_1(h,v) + (\lambda_v - \mu)g/W]/[2C_2(h,v)] \tag{C19}$$

and for bank angle control

$$H_u^* = H_u + \mu 2gD_2(h,v)u/W$$

(21) becomes

$$\nu = -\lambda_\psi W/[2(\lambda_v - \mu)D_2(h,v)v] \tag{C20}$$

Note in (C19) and in (C20) $\lambda_v - \mu$ can be replaced via (C18) by

$$\lambda_v - \mu = \lambda_h v/g \tag{C21}$$

We are now in a position to compare the solutions for the convex set with those of the "natural" set. If the latter solutions have a better performance we shall accept them, since the acceleration constraint was only artificially introduced to satisfy the minimum principle rather than representing passenger or equipment requirements. The above constraints, which only apply to the descent, did not affect the performance (less than 0.2 lb worse than the unconstrained optimal).

REFERENCES

1. Erzberger, H; and Lee, H. Q.: Algorithm for Fixed-Range Optimal Trajectories. NASA TP-1565, 1980.

2. Kreindler, Eliser; and Neuman, Frank: Global Optimality of Extremals: An Example. NASA TM-81240, 1980; also Journal of Optimization Theory and Applications, vol. 37, no. 4, Aug. 1982.

3. Erzberger, H.; and Lee, H. Q.: Terminal Area Guidance Algorithms for Automated Air Traffic Control. NASA TN D-6773, 1972.

4. Pecsvaradi, T.: Optimal Horizontal Guidance Law for Aircraft in the Terminal Area. IEEE Trans. Automat. Contr., vol. AC 17, no. 6, Dec. 1972.

5. McLean, J. D.: A New Algorithm for Horizontal Capture Trajectories. NASA TM-81186, 1980.

6. Kreindler, E.; and Neuman, F.: Minimum Fuel Horizontal Flightpaths in the Terminal Area. NASA TM-81313, 1981; also J. of Guidance, Control and Dynamics, vol. 5, no. 5, Sept.-Oct. 1982.

7. Lee, H. Q.; and Neuman, F.: 4D Area Navigation System Description and Flight Test Results. NASA TN D-7874, 1975.

8. McLean, J. D.; and Erzberger, H.: Design of a Fuel-Efficient Guidance System for a STOL Aircraft. NASA TM-81256, 1981.

9. Erzberger, H.: Automation of On-Board Flightpath Management. NASA TM-84212, 1981.

10. Bellman, R.: Dynamic Programming. Princeton University Press, Princeton, 1951.

11. Jacobson, D. H.; Lele, M. M.; and Speyer, J. L.: New Necessary Conditions of Optimality for Control Problems with State-Variable Inequality Constraints. J. Math. Anal. Appl., vol. 35, 1971, pp. 255-284.

12. Jacob, H. G.: An Engineering Optimization Method with Application to STOL-Aircraft Approach and Landing Trajectories, NASA TN D-6978, Sept. 1972.

13. Lee, E. B.; and Markers, L.: Foundations of Optimal Control Theory. Wiley and Sons, New York, 1967.

14. Schultz, Robert L.; and Zagalsky, Nelson R.: Aircraft Performance Optimization. J. of Aircraft, vol. 9, 1973, pp. 108-114.

1. Report No.	2. Government Accession No.	3. Recipient's Catalog No.
NASA TM-84289		

4. Title and Subtitle	5. Report Date
MINIMUM-FUEL TURNING CLIMBOUT AND DESCENT GUIDANCE OF TRANSPORT JETS	6. Performing Organization Code January 1983
7. Author(s)	8. Performing Organization Report No.
F. Neuman and E. Kreindler*	A-9067
9. Performing Organization Name and Address	10. Work Unit No.
NASA Ames Research Center Moffett Field, Calif. 94035	T-3309Y
	11. Contract or Grant No.
	13. Type of Report and Period Covered Technical Memorandum
12. Sponsoring Agency Name and Address	14. Sponsoring Agency Code
National Aeronautics and Space Administration Washington, D.C. 20546	505-34-11-11

15. Supplementary Notes

*Professor at E. E. Technion, Israel Institute of Technology, Haifa, Israel. Point of Contact: F. Neuman, Ames Research Center, M/S: 210-9, Moffett Field, Calif. 94035. (415) 965-5451 or FTS 448-5451.

16. Abstract

The complete flightpath optimization problem for minimum fuel consumption from takeoff to landing including the initial and final turns from and to the runway heading is solved. However, only the initial and final segments which contain the turns are treated, since the straight-line climbout, cruise, and descent problems have already been solved. The paths are derived by generating fields of extremals, using the necessary conditions of optimal control together with singular arcs and state constraints. Results show that the speed profiles for straight flight and turning flight are essentially identical except for the final horizontal accelerating or decelerating turns. The optimal turns require no abrupt maneuvers, and an approximation of the optimal turns could be easily integrated with present straight-line climb-cruise-descent fuel-optimization algorithms. Climbout at the optimal IAS rather than the 250-knot terminal-area speed limit would save 36 lb of fuel for the 727-100 aircraft.

17. Key Words (Suggested by Author(s))	18. Distribution Statement
Optimal guidance Minimum fuel Transport jet aircraft	Unlimited Subject Category - 08

19. Security Classif. (of this report)	20. Security Classif. (of this page)	21. No. of Pages	22. Price*
Unclassified	Unclassified	45	A03

*For sale by the National Technical Information Service, Springfield, Virginia 22161